9243

193

[redacted]

Copy
RM L54C04

[redacted]

NACA RM L54C04

7532

TECH LIBRARY KAFB, NM

0144338

NACA

RESEARCH MEMORANDUM

ROCKET-POWERED MODEL INVESTIGATION OF LIFT, DRAG, AND STABILITY OF A BODY-TAIL CONFIGURATION AT MACH NUMBERS FROM 0.8 TO 2.3 AND ANGLES OF ATTACK BETWEEN ±6.5°

By Warren Gillespie, Jr., and Albert E. Dietz

Langley Aeronautical Laboratory
Langley Field, Va.

[redacted]

NATIONAL ADVISORY COMMITTEE
FOR AERONAUTICS

WASHINGTON
April 15, 1954

[redacted]

[redacted]

TECH LIBRARY KAFB, NM
0144338

NATIONAL ADVISORY COMMITTEE FOR AERONAUTICS

RESEARCH MEMORANDUM

ROCKET-POWERED MODEL INVESTIGATION OF LIFT, DRAG, AND STABILITY OF A BODY-TAIL CONFIGURATION AT MACH NUMBERS FROM 0.8 TO 2.3 AND ANGLES OF ATTACK BETWEEN ±6.5°

By Warren Gillespie, Jr., and Albert E. Dietz

SUMMARY

A configuration having a body of fineness ratio 16.6, an unswept horizontal tail of aspect ratio 2.7, and a highly swept vertical tail was aeropulsed continuously in pitch during free flight with and without a sustainer rocket motor operating. The Mach number range covered by the test was 0.8 to 2.3 and the model angle of attack did not exceed ±6.5°. Zero-lift-drag and drag-due-to-lift data were obtained during coasting flight of the model. Normal-force, pitching-moment, and static-stability data were obtained with and without the rocket motor thrusting.

Correlation of power-off normal-force- and pitching-moment-curve slopes with theoretical estimates based on slender-body theory as presented in NACA RM A52D29 gives good agreement with experiment. The reciprocal of the normal-force-curve slope closely approximates experimental drag-due-to-lift values. The amplitude of the angle-of-attack oscillations during flight with power on was approximately 50 percent smaller than the amplitude during coasting flight, and the normal-force- and pitching-moment-curve slopes were effectively higher during powered flight. The above differences between coasting and powered-flight values may be largely due to cross-coupling effects induced by operation of the sustainer rocket motor and the asymmetry of the cruciform tail.

INTRODUCTION

As part of a general program to determine the aerodynamic characteristics of wing-body-tail combinations at supersonic speeds and moderate angles of attack, a body-tail configuration was flight-tested

[redacted]

at the Langley Pilotless Aircraft Research Station, Wallops Island, Va. The aeropulse technique as presented in reference 1 and a large solid-fuel sustainer rocket motor were used to obtain lift, drag, and static stability of the model at Mach numbers from 0.8 to 2.3 and angles of attack up to $\pm 6.5^{\circ}$. The model consisted of a body of fineness ratio 16.6 with an unswept horizontal pulsing tail of aspect ratio 2.7 and a highly swept fixed vertical tail of aspect ratio 1.08. The horizontal tail was aerodynamically actuated between stop settings of $\pm 2.0^{\circ}$ in approximately a square-wave pattern with a frequency of from 2 to 5 cycles a second. The basic aerodynamic parameters in pitch were determined from the response of the model to the tail motion.

SYMBOLS

C_N	normal-force coefficient, $\frac{a_n}{g}\frac{W/S}{q}$
C_c	chord-force coefficient, $-\frac{a_l}{g}\frac{W/S}{q}$
C_D	drag coefficient, $C_c \cos \alpha + C_N \sin \alpha$
C_m	pitching-moment coefficient, $\frac{I_y\ddot{\theta}}{57.3qSd}$
a_n	normal acceleration, ft/sec^2
a_l	longitudinal acceleration, ft/sec^2
g	acceleration due to gravity, 32.2 ft/sec^2
q	dynamic pressure, lb/sq ft
M	Mach number
R	Reynolds number, where the reference length is 1 ft
S	body cross-sectional area, 0.267 sq ft
d	body diameter, 0.583 ft
α	angle of attack, deg
θ	angle of pitch, deg

[redacted]

ψ	angle of yaw, deg
p	roll rate, radians/sec
δ	all-movable horizontal-tail deflection, $\pm 2.0^{\circ}$
ϵ	effective upwash at the tail, deg
I_Y	moment of inertia about Y-axis, slug-ft^2
I_X	moment of inertia about X-axis, slug-ft^2
I_Z	moment of inertia about Z-axis, slug-ft^2
P	rocket chamber pressure, lb/sq in. abs
T	rocket motor thrust, lb
t	time, sec
x	distance from center of pressure to model base, in.
l	model length, 116.13 in.
m	model mass, slug

Subscripts:

g	ground
f	flight

Note: One and two dots over symbols denote first and second time derivatives, respectively.

MODEL

A two-view drawing of the test configuration is shown in figure 1. The fuselage was a body of revolution of fineness ratio 16.6. Ordinates defining the nose shape are given in table I. The geometric and mass characteristics are listed in table II, and photographs are shown in figure 2. The maximum body-diameter-tail-span ratio was 0.350 for the vertical tail and 0.315 for the horizontal tail. The horizontal tail was mass-balanced and pivoted $\pm 2.0^{\circ}$ about the 0.55-exposed-mean-aerodynamic-chord point.

The model was of metal construction and carried a solid-fuel sustainer rocket motor in addition to an eight-channel telemeter with angle-of-attack, pressure, and accelerometer instruments.

The model and its booster are pictured in the launching attitude in figure 3. Total impulse was approximately 17,000 lb-sec for the solid-fuel Deacon booster and 7,660 lb-sec for the sustainer motor.

TEST

Data were obtained after the model separated from the booster. During flight of the model alone, a square-wave pulse was continuously generated as the tail automatically flipped between stop settings due to a reversal in direction of the tail lift.

The quantities measured by the telemeter system were normal and longitudinal accelerations, angle of attack, horizontal-tail position, free-stream total pressure, and sustainer-rocket-chamber pressure. The angle-of-attack indicator mounted on the vertical tail became inoperative before sufficient data could be recorded. The velocity obtained from Doppler radar was used in conjunction with tracking radar and radiosonde data to calculate Mach number, Reynolds number, and dynamic pressure experienced by the model during flight. The variation of Reynolds number per foot length and dynamic pressure with Mach number are shown in figure 4. The model experienced a coasting period before and after the period of flight with the sustainer motor thrusting.

Aerodynamic coefficients were determined for coasting and power-on flight conditions. Data at a particular Mach number were obtained only during constant tail deflections of $\pm 2.0^{\circ}$. Coefficients are based on the body maximum cross-sectional area of 0.267 square foot and on the body diameter of 0.58 foot. A detailed explanation of data analysis is given in reference 1. Pitching moment was determined from the difference in normal accelerations measured at the nose and near the center of gravity of the model.

ACCURACY

The random error in the data is indicated by the scatter of the experimental points which is generally much less at the highest Mach numbers. The maximum absolute accuracy of a quantity obtained from a single instrument is usually better than 2 percent of the total calibrated instrument range. The probable error is approximately 1 percent. Presented on the following page are the ranges of the telemeter instruments used in the test model:

Nose angle-of-attack indicator, deg	±8
Normal accelerometer at the nose, g-units	±8
Normal accelerometer near the center of gravity, g-units	±20
Longitudinal accelerometer, coasting, g-units	1 to -7
Longitudinal accelerometer, power on, g-units	-5 to 60
Rocket chamber pressure, lb/sq in.	0 to 1400
Free-stream total pressure, lb/sq in.	-5 to 115

An additional source of inaccuracy in the final results may be cross-coupling effects of induced rolling and yawing motion. This possibility is discussed more thoroughly in a later section.

RESULTS AND DISCUSSION

Model pitching response.- Typical portions of the pitching response of the model are shown in figures 5, 6, and 7. Figure 5 shows a part of the decelerating flight time history of the first coasting period and indicates how the model angle of attack, normal acceleration, and Mach number varied as the tail moved in an approximate square-wave pattern of ±2.0° deflection. Figure 6 shows portions of the angle-of-attack telemeter record throughout the flight of the model after separation from the booster. The aeropulse motion developed immediately after the model became free of the booster. The oscillations during the first coast period were uniformly symmetrical. The record shows that the angle-of-attack indicator at the tail started to vibrate at Mach number 1.2 and then ceased to function. The record also shows that the amplitude of the sinusoidal oscillations was suddenly reduced and varied after the sustainer motor started thrusting. Figure 7 shows more clearly that the amplitude of the angle-of-attack oscillations was reduced approximately 50 percent during operation of the sustainer motor. After sustainer burnout the oscillations increased in amplitude but were asymmetrical during the early part of the second coasting period and irregular during the latter part.

Cross coupling.- The curious variations that occurred in the angle-of-attack response of the test model may be largely due to cross-coupling effects of rolling and yawing motions. Such motions may have been instigated by operation of the sustainer rocket motor and amplified by the asymmetry of the horizontal-tail and vertical-tail plan forms and horizontal-tail deflections of ±2.0°. At the time of sustainer ignition, it is estimated that thrust misalinement in yaw could have started a yawing motion with an initial maximum yaw angle of approximately two times the amount of angular thrust offset. A thrust offset of approximately 0.4° in pitch is estimated from the trim offset indicated by figure 7. From reference 2 it may be determined that the value of the rolling parameter C_{l_β}/α for the horizontal tail of the test model is

small compared with that for the vertical tail. The test model therefore may have experienced an aerodynamic rolling moment at combined angles of pitch and yaw. This is different from the case of a symmetrical cruciform missile for which the rolling tendencies of the individual tail surfaces would cancel at angles of attack up to about 6°, as shown by the experimental data of reference 3.

An investigation of the effect of steady rolling on longitudinal and directional stability was reported in reference 4 where the stability was studied by means of the Euler moment equations. In particular the equation for pitching moment $M = I_Y\ddot{\theta} - (I_Z - I_X)\dot{\psi}p$ shows the term introduced by the combination of rolling and yawing velocity. This moment term may have affected the pitching moment measured by the accelerometers of the test model. The accelerometer measuring normal force may have been similarly affected by a term containing the product of yaw angle and roll velocity as shown by the following expression

$$Z = mV(\dot{\alpha} - \dot{\theta}) - mV\psi p$$

Calculations were therefore made to determine the possible effect of cross coupling on the transient angle-of-attack response of the test model. The method of calculation is given in appendix A. The results of these calculations are shown in figure 8 and indicate that for reasonable values of roll rate and initial yawing velocity cross coupling probably caused the asymmetrical pitching oscillations of the second coasting period. Cross coupling may also have been largely responsible for reducing the amplitude of oscillation during powered flight. Additional calculations made without cross-coupling terms show that during the second coasting period when the tail setting was -2.0° the experimental oscillation can be very exactly matched by the calculation method of reference 1. During part of the second coasting period, therefore, the effect of cross coupling on the pitching motion was apparently negligible.

Sustainer motor.- Operation of the sustainer rocket motor in flight was not appreciably affected by the high longitudinal and normal flight accelerations encountered. This is shown in figure 9 where the rocket chamber pressure obtained during a static ground test is compared with the chamber pressure measured in flight. Thrust during flight was calculated from the expression $T_f = T_g(P_f/P_g)$ where the values used occurred at corresponding burning times during the ground and flight tests. Thrust corrections to account for differences in back pressure during the ground and flight tests were negligible.

The effect of the thrust lift component $T \sin \alpha$ on the amplitude of the pitching response during powered flight was also considered. The method of calculation is given in appendix B. The calculation

shows that the thrust lift component probably reduced the power-on pitching amplitude approximately 14 percent below the amplitude without thrust acting.

Angle of attack at zero normal force and at tail flip.- Figure 10 shows the angle of attack at the instant the model pitched through zero normal force during coasting and powered flight. The dashed line is interpolated for a tail setting of 0° and lies close to zero angle of attack in the low supersonic range. As the Mach number approached 2.0, the angle of attack for $C_N = 0$ changed approximately 0.5°. The angle-of-attack indicator had a 60° delta surface. It is probable that the indicator changed trim as the flow velocity normal to the leading edge of the indicator surface changed from subsonic to supersonic velocity at Mach number 2.0. The trim effect of small pressure disturbances arising from minute imperfections in the construction of the indicator would probably be different, depending on whether the leading edge was subsonic or supersonic.

The angle of attack at the instant that the horizontal tail started to flip from one stop setting to the other is presented in figure 11. Assuming that at this instant the effective angle of attack at the tail was zero, the effective upwash at the tail can be approximately estimated from the relation

$$\epsilon = -\alpha_{flip} - \delta$$

The average effective upwash over the tail obtained from the two tail settings was 1.1° at an average angle of attack of 0.9° over the Mach number range of the tests. This is greater than would be expected from two-dimensional potential-flow theory and the experimental data of figure 30 of reference 5. The high upwash indicated by the tail flipping may be due to the degree of mass balance of the tail which could affect the start of the tail flipping.

Drag.- A typical drag polar is presented in figure 12. The polar is composed of data from one oscillation with tail settings of $\pm 2.0^{\circ}$. The drag characteristics are summarized in figure 13 which shows the variation of zero-lift drag and drag due to lift with Mach number. The zero-lift drag coefficient reached a peak value of 0.52 at Mach number 1.0 for this configuration and uniformly decreased at higher Mach numbers. The drag due to lift had a minimum value of 0.046 at Mach number 1.0 and increased with increasing Mach number. The parameter $\frac{1}{57.3C_{N_\alpha}}$ is in good agreement with drag-due-to-lift values.

Normal force, pitching moment, and tail effectiveness.- Figures 14 to 18 present typical plots of normal-force and pitching-moment coefficients

and summarize the variation of the normal-force- and pitching-moment-curve slopes with Mach number. The unusual variation of the normal force and pitching moment with angle of attack exhibited in figure 15 for a tail setting of 2.0° occurred during the asymmetrical oscillations of the second coasting period. The change in slope of these curves between points B to D may be due to cross-coupling effects of induced rolling and yawing motions during this portion of the oscillation. Slopes obtained between points D to E and F to A were used in preparation of figures 16 and 17. Figures 16 and 17 show that the normal-force- and pitching-moment-curve slopes due to angle of attack were effectively higher during powered flight than during coasting flight. The increase in these slope values between powered and coasting flight is of the same magnitude as that indicated by regions B to D of figure 15. It appears therefore that the cross-coupling terms $mV\psi p$ and $(I_Z - I_X)\psi p$ discussed previously may have caused the differences between coasting and powered-flight values.

Figure 16 also shows the tail lift effectiveness. No difference between power-on and power-off values of this parameter can be determined because of the rather large scatter of the data.

Figure 18 presents a comparison of normal-force-curve slope and tail effectiveness with the theory of reference 6. Very good agreement is noted for the normal-force-curve slope at all Mach numbers and the tail effectiveness at the highest Mach numbers of the test.

Model aerodynamic center.- Figure 19 shows the variation of model aerodynamic center with Mach number for both power-off and power-on flight conditions. There is very little difference due to power effects. The most rearward power-off location of the aerodynamic center at 21 percent body length from the base occurred near Mach number 1.0. At higher Mach numbers the aerodynamic center moved uniformly forward as the tail effectiveness decreased. Figure 20 compares aerodynamic-center location calculated by the method of reference 6 with the experimental curve of the present test. Using the first-order theory of reference 7 to determine the nose contribution rather than slender-body theory gives very good agreement between the curves.

Induced jet effect.- The possibility of induced jet effects on the powered-flight values of C_{N_α}, C_{m_α}, and aerodynamic-center location was also considered. However, reference 8 shows that induced jet effects on the afterbody of a rocket model would not be expected to occur above a Mach number of 1.4. Below Mach number 1.4 strong jet effects would probably not extend more than 1 base diameter forward of the jet exit. The horizontal tail of the test model was located over 1 base diameter ahead of the jet exit. Furthermore, if induced jet effects at the model tail had caused the C_{N_α} and C_{m_α} slope differences shown in figures 16

and 17, then the model aerodynamic center should have shifted farther rearward than the small amount shown in figure 19. It seems probable that large induced jet effects were not present.

CONCLUSIONS

An investigation of lift, drag, and stability of a rocket-propelled body-tail configuration between Mach numbers of 0.8 and 2.3 with and without the sustainer motor operating leads to the following conclusions:

1. During coasting flight, the drag due to lift increased with increasing Mach number throughout the supersonic range of the test and was slightly higher than the reciprocal of the normal-force-curve slope. The lift and aerodynamic-center location were accurately predicted by use of the interference factors derived from slender-body theory.

2. The amplitude of the pitching oscillations was smaller during powered flight and the normal-force- and pitching-moment-curve slopes were effectively higher than values obtained during coasting flight. These differences may be largely due to cross-coupling effects induced by operation of the sustainer rocket motor and the asymmetry of the cruciform tail.

Langley Aeronautical Laboratory,
National Advisory Committee for Aeronautics,
Langley Field, Va., February 18, 1954.

APPENDIX A

EFFECT OF CROSS COUPLING ON TRANSIENT ANGLE OF ATTACK

The calculation of the effect of cross coupling on the transient angle-of-attack response to a step input tail deflection of the test model was made in the following manner. In order to simplify the calculations, only angular motions in pitch and yaw were considered. Aerodynamic damping was neglected. The aerodynamic moments for equal angles of pitch and yaw were assumed equal. The model inertia about the longitudinal axis was assumed zero and roll rate was assumed constant. The moment equations in pitch and yaw with axes fixed in the model reduced to

$$\frac{I_Y}{57.3}\ddot{\alpha} - \frac{I_Y}{57.3}p\dot{\psi} - C_{m_\alpha}\alpha qSd = C_{m_\delta}\delta qSd$$

$$\frac{I_Z}{57.3}\ddot{\psi} + \frac{I_Z}{57.3}p\dot{\alpha} - C_{m_\alpha}\psi qSd = 0$$

or, since $I_Y = I_Z$ for the test model,

$$A\ddot{\alpha} - B\dot{\psi} - C\alpha = k$$

$$A\ddot{\psi} + B\dot{\alpha} - D\psi = 0$$

and $\alpha_{trim} = -\frac{k}{C}$ and $p = \frac{B}{A}$. The solution with no damping is

$$\alpha(t) = \alpha_{trim} + \frac{2C_1a_1^4 - 2C_3a_1^2 + 2C_5}{5a_1^4 - 3C_6a_1^2 + C_7}\cos 57.3a_1t +$$

$$\frac{2C_2a_1^3 - 2C_4a_1}{5a_1^4 - 3C_6a_1^2 + C_7}\sin 57.3a_1t + \frac{2C_1a_2^4 - 2C_3a_2^2 + 2C_5}{5a_2^4 - 3C_6a_2^2 + C_7}\cos 57.3a_2t +$$

$$\frac{2C_2a_2^3 - 2C_4a_2}{5a_2^4 - 3C_6a_2^2 + C_7}\sin 57.3a_2t$$

where

$$a_1^2 = \frac{C_6}{2} - \sqrt{\left(\frac{C_6}{2}\right)^2 - C_7}$$

$$a_2^2 = \frac{C_6}{2} + \sqrt{\left(\frac{C_6}{2}\right)^2 - C_7}$$

$$C_1 = \alpha(0)$$

$$C_2 = \dot{\alpha}(0)$$

$$C_3 = p\dot{\psi}(0) - \frac{D}{A}\alpha(0) + p^2\alpha(0) + \frac{k}{A}$$

$$C_4 = p\frac{D}{A}\psi(0) - \frac{D}{A}\dot{\alpha}(0)$$

$$C_5 = -\frac{kD}{A^2}$$

$$C_6 = p^2 - \frac{C}{A} - \frac{D}{A}$$

$$C_7 = \frac{DC}{A^2}$$

APPENDIX B

EFFECT OF THRUST LIFT COMPONENT ON MAXIMUM AEROPULSE ANGLE OF ATTACK

The effect of the thrust lift component $T \sin \alpha$ on the maximum aeropulse angle-of-attack response was calculated using the logarithmic chart of figure 21. The chart was originally derived by Mr. Robert L. Nelson of the NACA Langley Pilotless Aircraft Research Division and is based on the equations of longitudinal motion with freedom in pitch about the y-axis and translation in the z-direction. In the derivation of the chart the assumptions of instantaneous tail flipping and equal but opposite slopes at succeeding times, t_0, t_1, . . ., of tail flip are made.

The solution for the maximum aeropulse response is

$$\frac{\alpha_m}{\alpha_{trim}} = 1 - \left(1 - \frac{\alpha_{flip}}{\alpha_{trim}}\right)e^{-bt_m}\left(\frac{b}{a} \sin 57.3at_m + \cos 57.3at_m\right) - \frac{\left(1 - \frac{\alpha_{flip}}{\alpha_{trim}}\right)\left(1 + \frac{b^2}{a^2}\right)e^{-b(t_m+t_1)}\sin 57.3at_m \sin 57.3at_1}{1 + e^{-bt_1}\left(\cos 57.3at_1 - \frac{b}{a} \sin 57.3at_1\right)}$$

and

$$\frac{(a_n)_m}{g} = \frac{qS}{W}\left(C_{N_\delta}\delta + C_{N_\alpha}\alpha_m\right)$$

where

$$\alpha_{trim} = -\frac{\frac{mV}{57.3qS} C_{m_\delta}\delta + C_{m_{\dot{\theta}}} \frac{d}{2V} C_{N_\delta}\delta}{C_{m_{\dot{\theta}}} \frac{d}{2V} C_{N_\alpha} + \frac{mV}{57.3qS} C_{m_\alpha}}$$

$$\alpha_{flip} \approx -\epsilon - \delta$$

$$a = \left[- \frac{57.3qS}{I_Y}\left(C_{m_\alpha} d + \frac{C_{N_\alpha} C_{m_{\dot{\theta}}} 57.3qSd^2}{2mV^2}\right) - b^2 \right]^{1/2}$$

$$b = \frac{57.3qS}{2}\left[\frac{C_{N_\alpha}}{mV} - \frac{\left(C_{m_{\dot{\theta}}} + C_{m_{\dot{\alpha}}}\right)d^2}{2VI_Y}\right]$$

$$t_m = \frac{1}{a} \tan^{-1} \frac{e^{-bt_1} \sin 57.3at_1}{1 + e^{-bt_1} \cos 57.3at_1}$$

Note that t_1 is the time at the tail flip following the previous maximum amplitude at the time t_m.

REFERENCES

1. Gillespie, Warren, Jr., and Dietz, Albert E.: Use of an Aerodynamically Pulsed All-Movable Horizontal Tail To Obtain Longitudinal Characteristics of Rocket-Powered Models in Free Flight and Some Initial Results From an Arrow-Wing-Body-Tail Configuration. NACA RM L52C10, 1952.

2. Jones, Arthur L., Spreiter, John R., and Alksne, Alberta: The Rolling Moment Due to Sideslip of Triangular, Trapezoidal, and Related Plan Forms in Supersonic Flow. NACA TN 1700, 1948.

3. Krenkel, A. R.: Generalized Missile Study First Annual Report. Rep. No. CF-1996, McDonnell Aircraft Corp., May 29, 1953.

4. Phillips, William H.: Effect of Steady Rolling on Longitudinal and Directional Stability. NACA TN 1627, 1948.

5. Spahr, J. Richard, and Dickey, Robert R.: Wind-Tunnel Investigation of the Vortex Wake and Downwash Field Behind Triangular Wings and Wing-Body Combinations at Supersonic Speeds. NACA RM A53D10, 1953.

6. Nielsen, Jack N., Kaattari, George E., and Drake, William C.: Comparison Between Prediction and Experiment for All-Movable Wing and Body Combinations at Supersonic Speeds - Lift, Pitching Moment, and Hinge Moment. NACA RM A52D29, 1952.

7. Van Dyke, Milton D.: First- and Second-Order Theory of Supersonic Flow Past Bodies of Revolution. Jour. Aero. Sci., vol. 18, no. 3, Mar. 1951, pp. 161-178.

8. Gillespie, Warren, Jr.: Jet Effects on Pressures and Drag of Bodies. NACA RM L51J29, 1951.

TABLE I.- CONTOUR ORDINATES OF NOSE

Station, in. from nose	Body radius, in.
0	0.17
.06	.18
.12	.21
.24	.22
.48	.28
.73	.35
1.22	.46
2.00	.64
2.45	.73
4.80	1.24
7.35	1.72
8.00	1.85
9.80	2.15
12.25	2.50
13.12	2.61
14.37	2.75
14.70	2.78
17.15	3.01
19.60	3.22
22.05	3.38
24.50	3.50
25.00	3.50

TABLE II.- CHARACTERISTICS OF MODEL

Body:	
Maximum diameter, ft	0.58
Base diameter, ft	0.42
Length, ft	9.68
Body fineness ratio	16.60
Nose fineness ratio	3.57
Boattail fineness ratio	3.86
Boattail angle, deg	2.16
Horizontal tail:	
Span, total, ft	1.85
Exposed area, sq ft	0.80
Aspect ratio, total span and area	2.70
Aspect ratio, exposed span and area	2.28
Taper ratio, exposed	0.40
Sweepback at 0.5c, deg	0
Airfoil section	4-percent hexagonal
Vertical tail:	
Span, total, ft	1.67
Chord at center line	2.73
Aspect ratio, total span and area	1.08
Sweepback at L.E., deg	70
Sweepback at T.E., deg	15
Airfoil section	1/4-inch beveled flat plate
Model weight, lb:	
With sustainer rocket loaded	183.6
With sustainer rocket empty	144.9
Moment of inertia in pitch or yaw, slug-ft^2:	
With sustainer rocket loaded	40.4
With sustainer rocket empty	37.5
Center of gravity with sustainer rocket loaded or empty, percent length from base	43.2

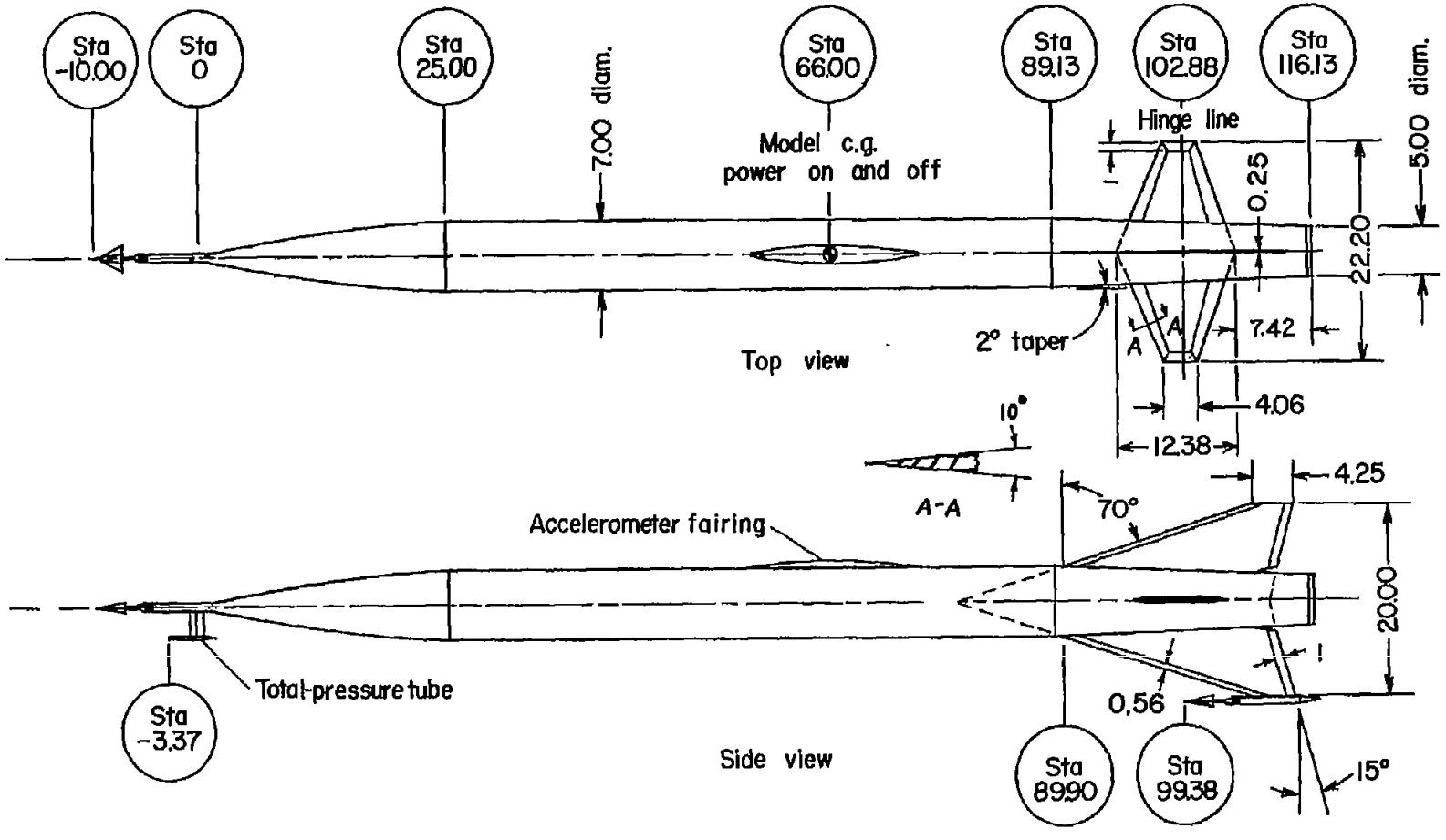

Figure 1.- Two-view drawing of the test configuration. All dimensions are in inches.

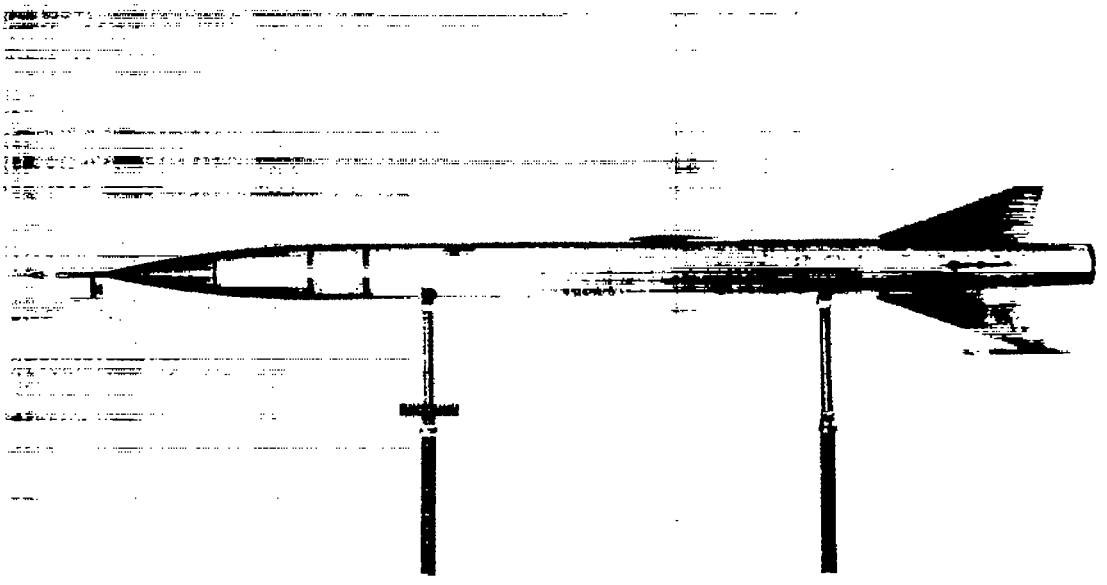

(a) Side view.

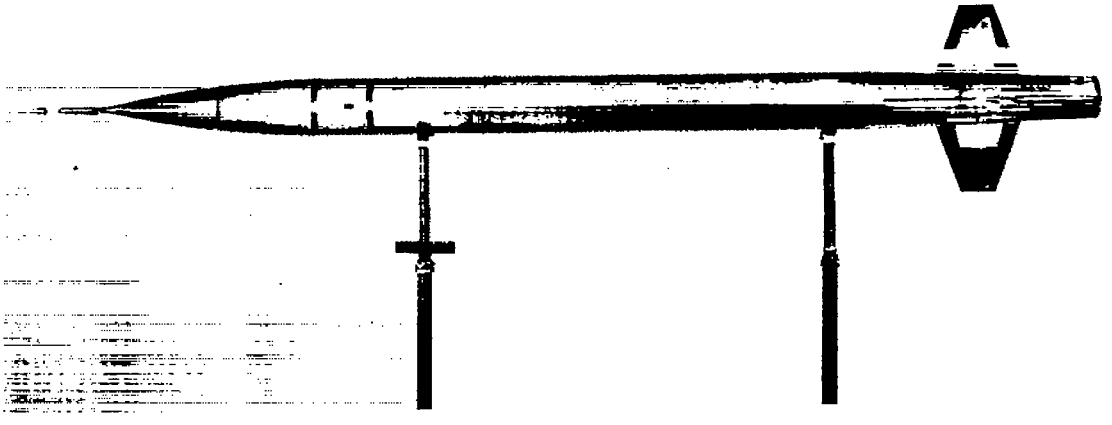

L-83335

(b) Bottom view.

Figure 2.- Photographs of test configuration.

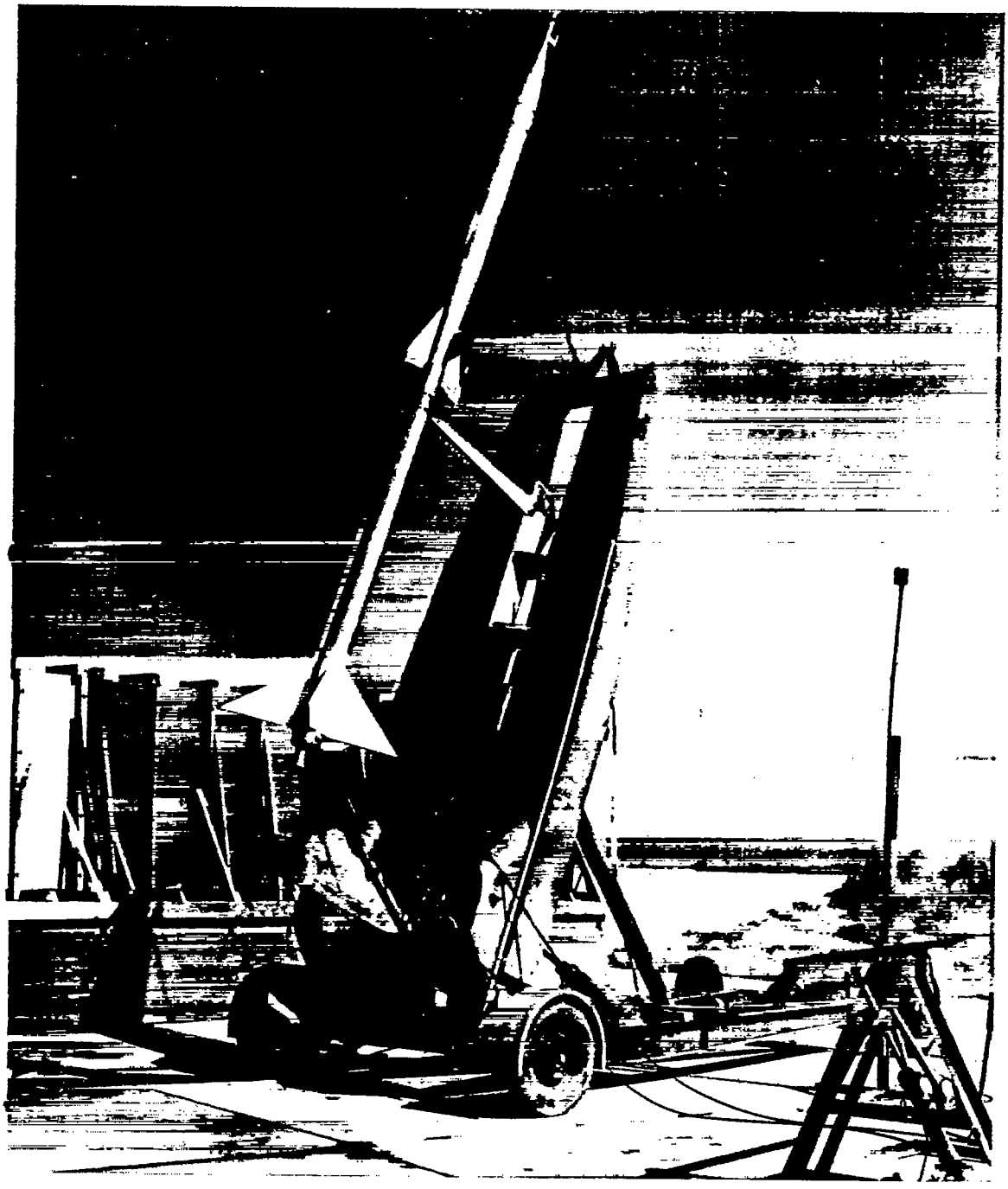

L-77377.1

Figure 3.- Model and booster on launcher.

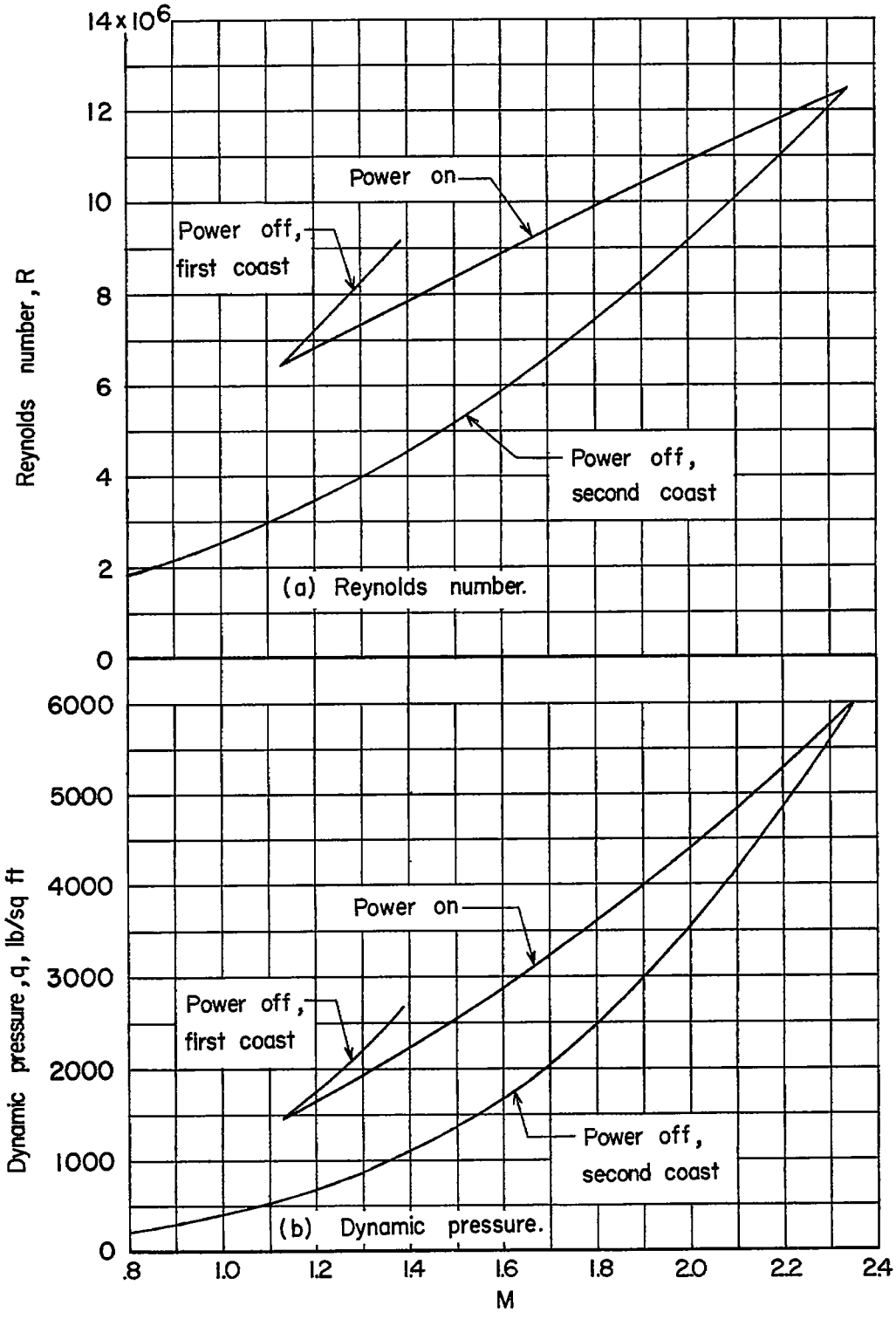

Figure 4.- Variation of Reynolds number and dynamic pressure with Mach number.

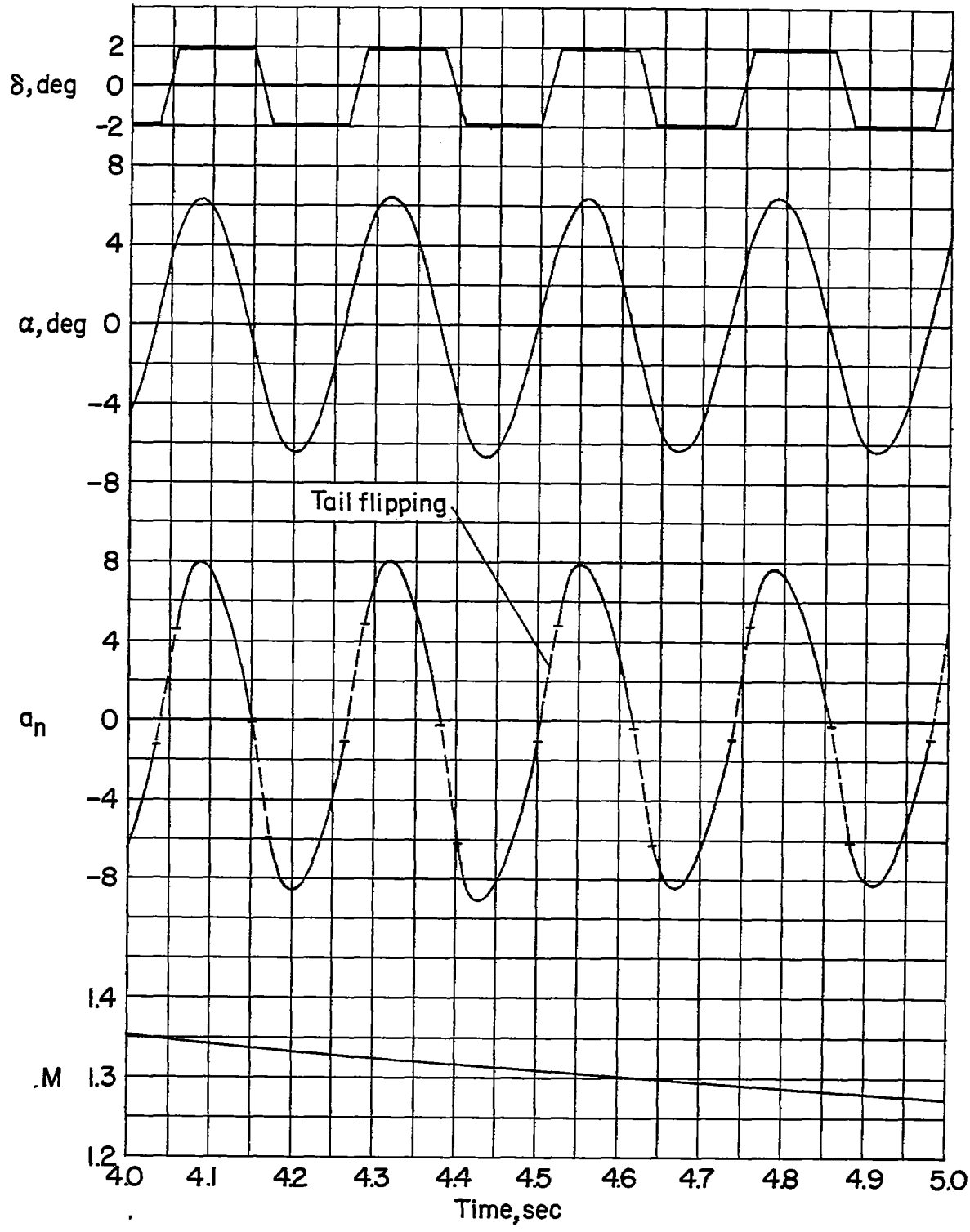

Figure 5.- A typical portion of the flight time history.

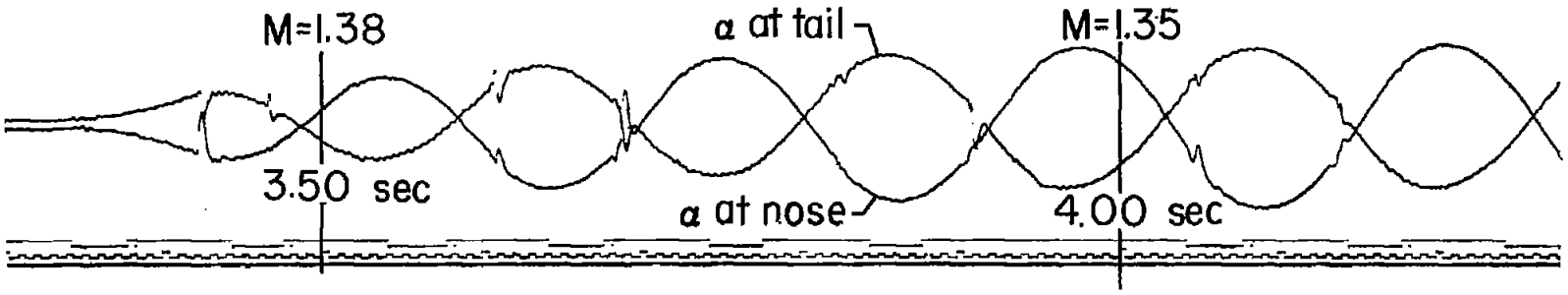

(a) Development of sinusoidal oscillation following model separation from booster.

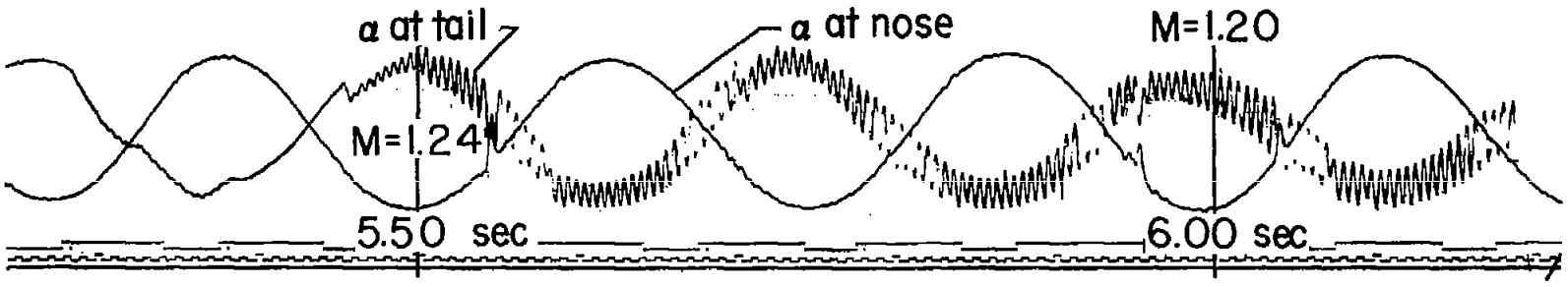

(b) Flutter of indicator at tail; M=1.24.

Figure 6.- Typical angle-of-attack oscillations during flight of model.

[redacted]

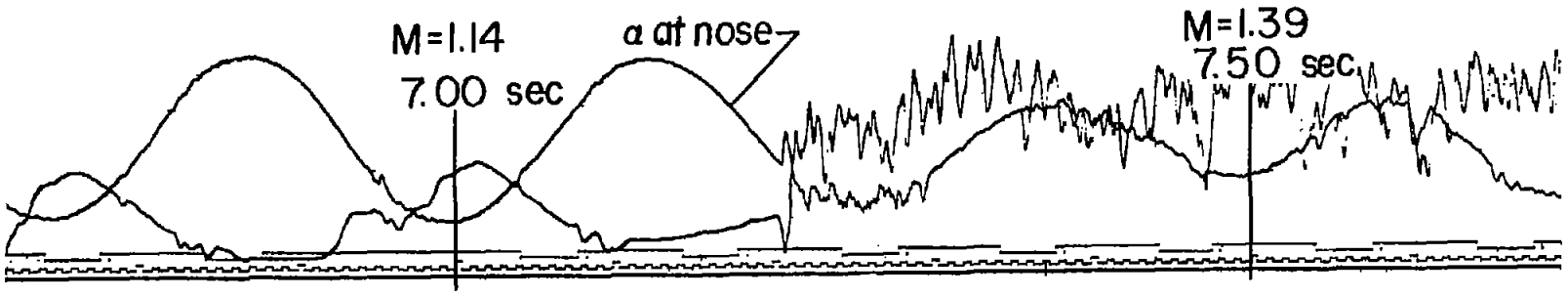

(c) Reduction in amplitude following ignition of sustainer motor at 7.2 seconds flight time.

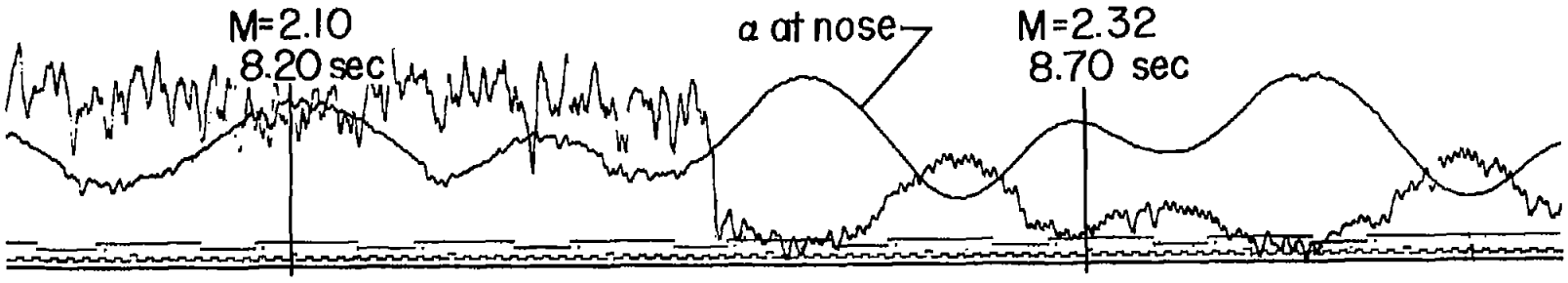

(d) Asymmetrical oscillations of increased amplitude following burnout at 8.4 seconds flight time.

Figure 6.- Continued.

[redacted]

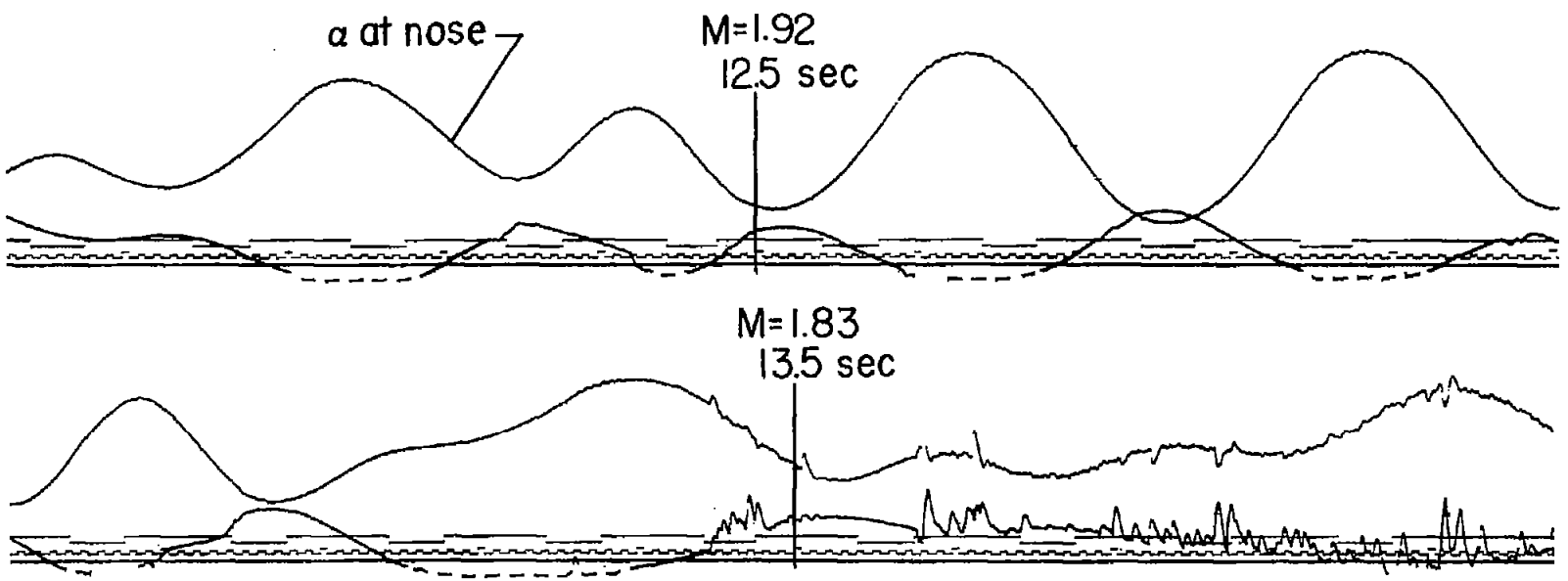

(e) Transition to irregular oscillations of varying amplitude.

Figure 6.- Concluded.

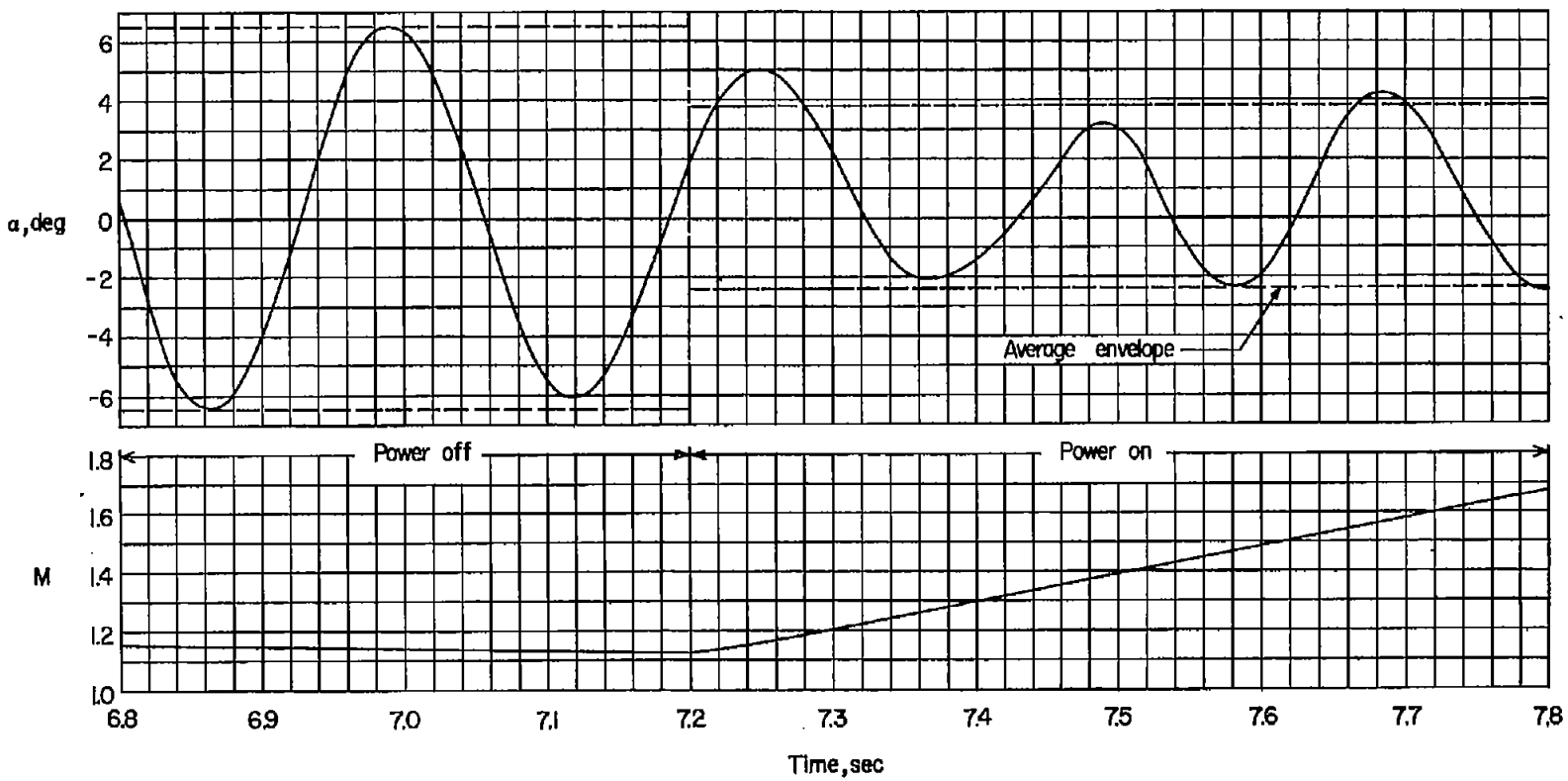

Figure 7.- Effect of powered flight on model angle of attack.

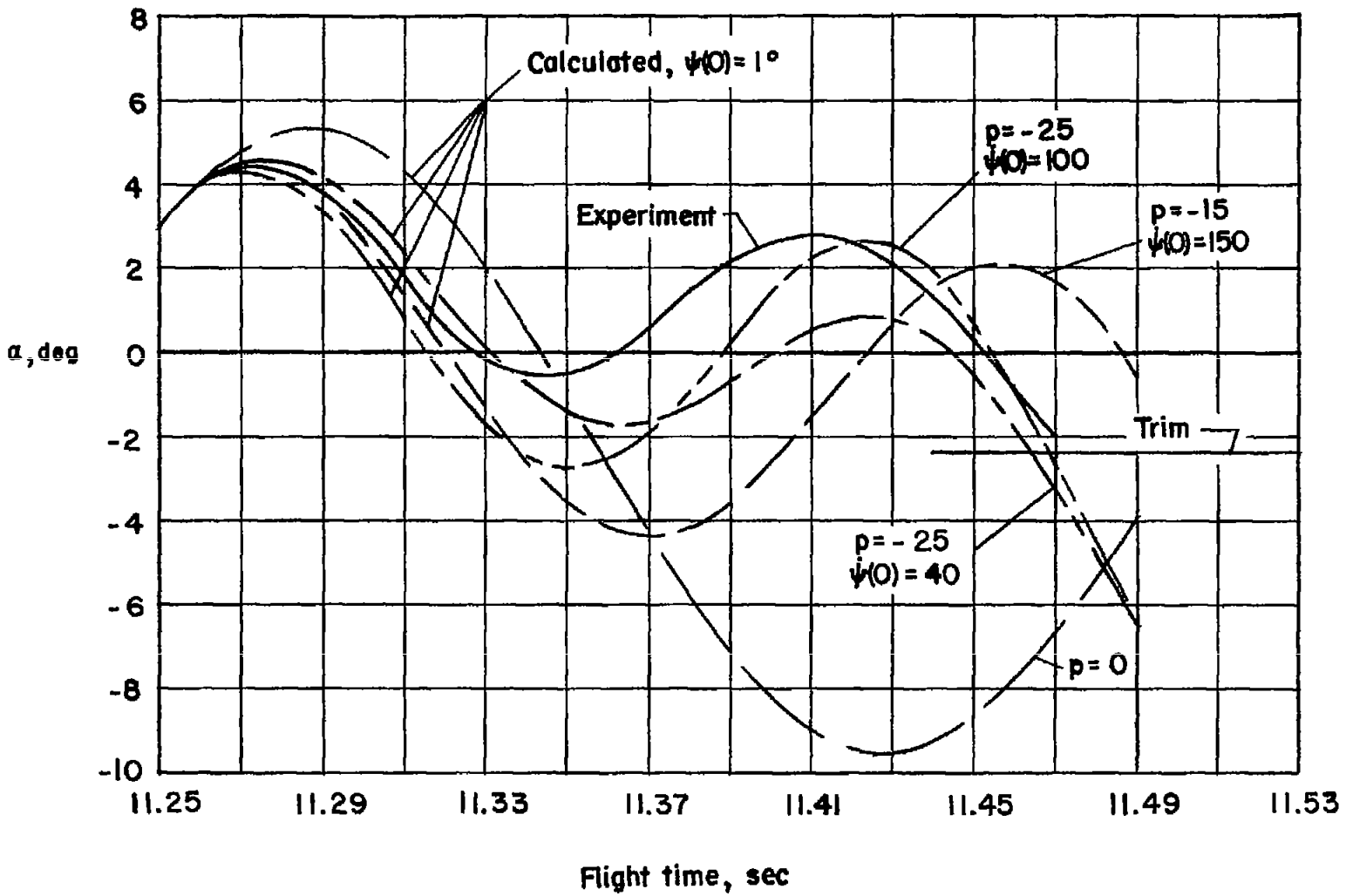

Figure 8.- Effect of constant roll and initial yaw rates on angle-of-attack response to tail deflection of 2.0°. M = 2.02.

[redacted]

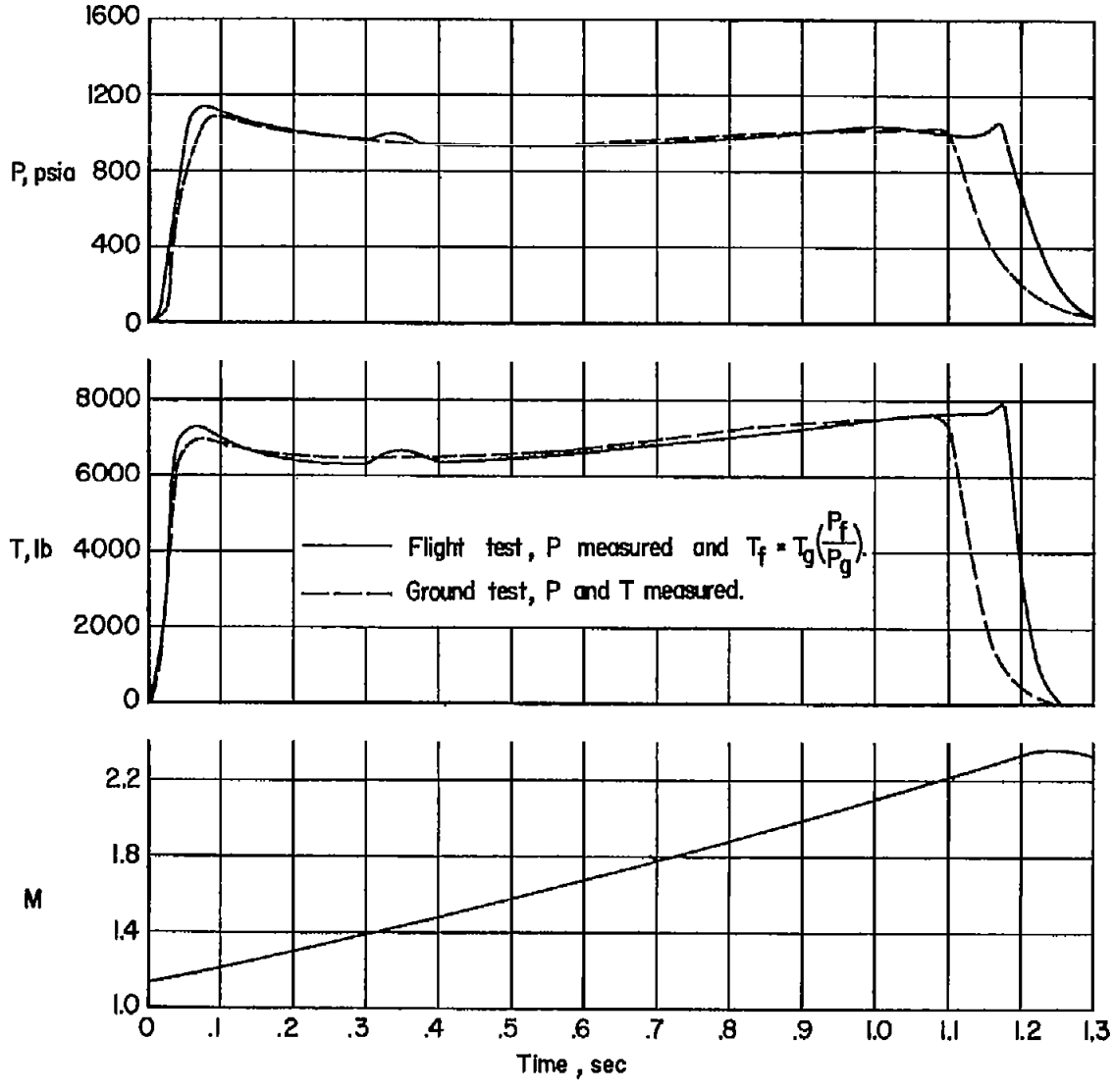

Figure 9.- Comparison of thrust developed during ground and flight tests.

[redacted]

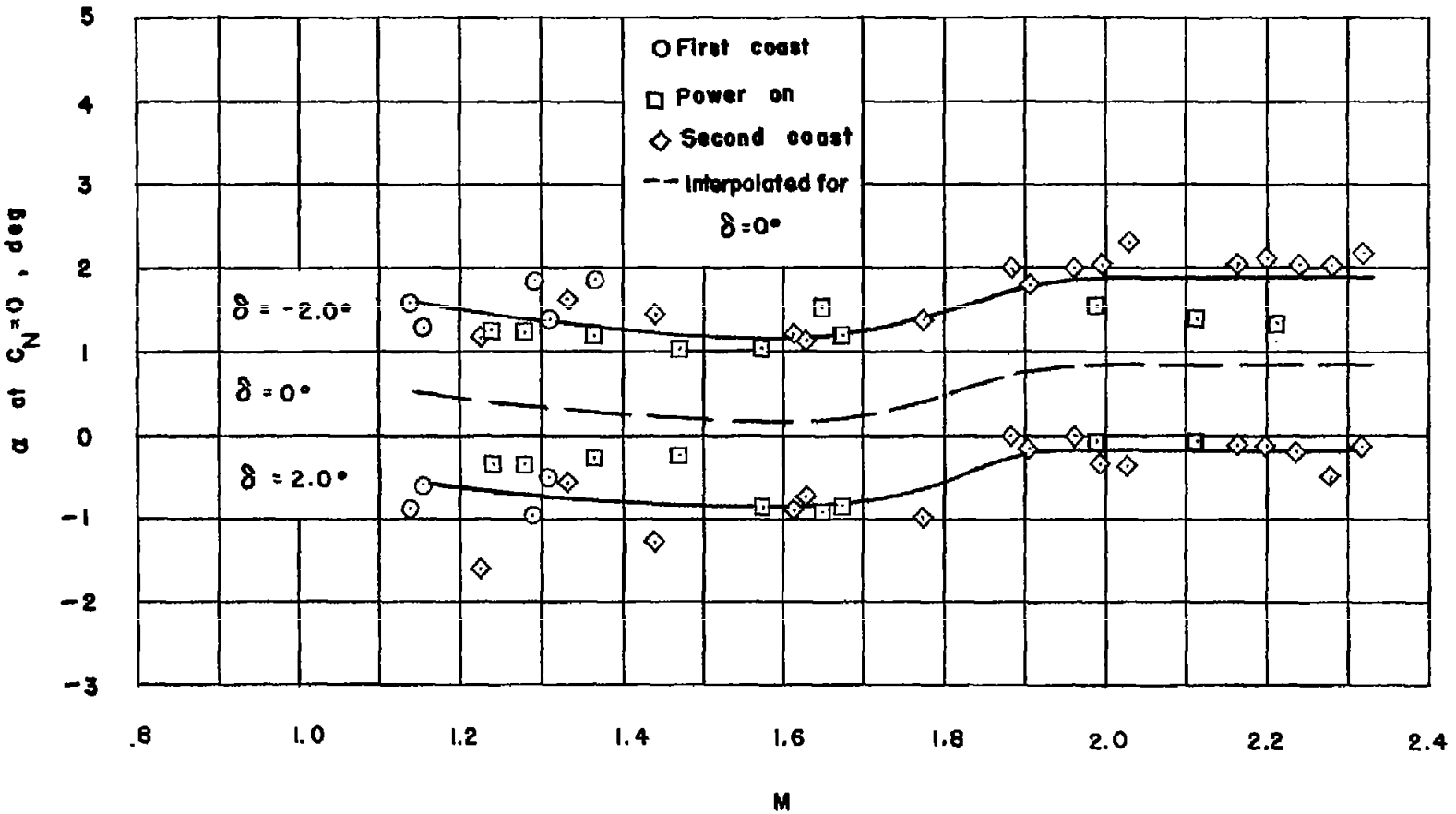

Figure 10.- Angle of attack at $C_N = 0$.

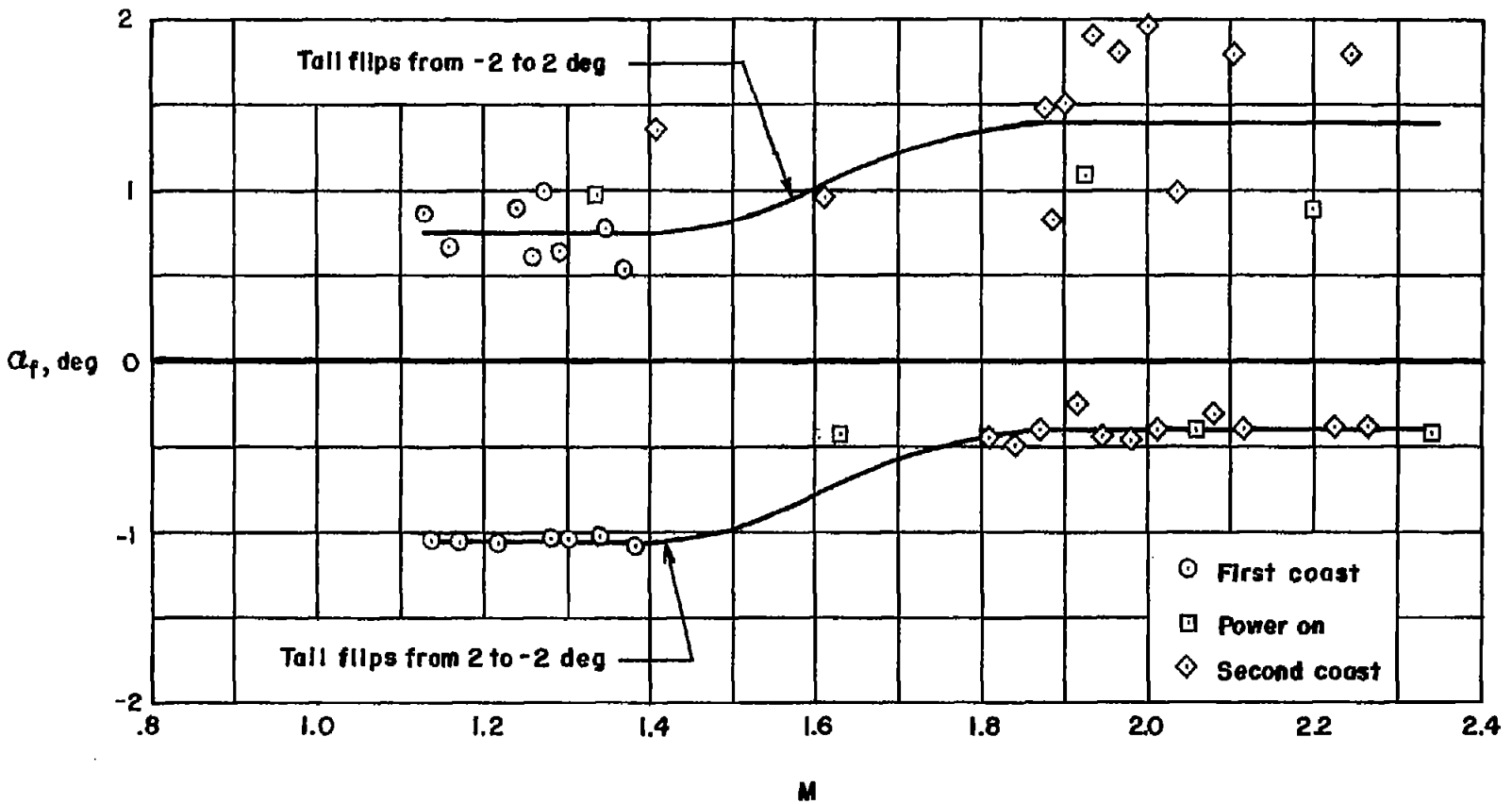

Figure 11.- Model angle of attack at tail flipping.

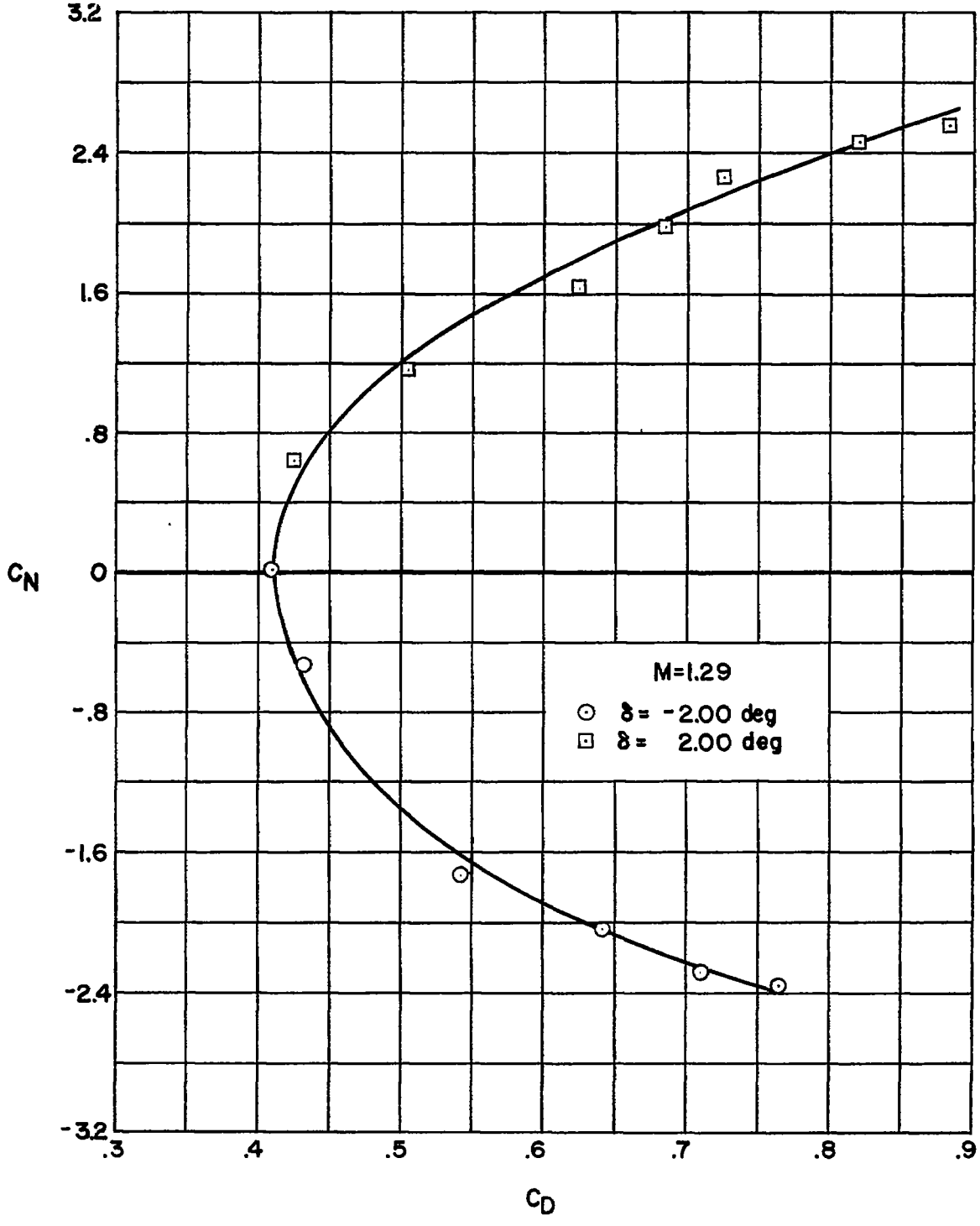

Figure 12.- A typical drag polar.

[redacted]

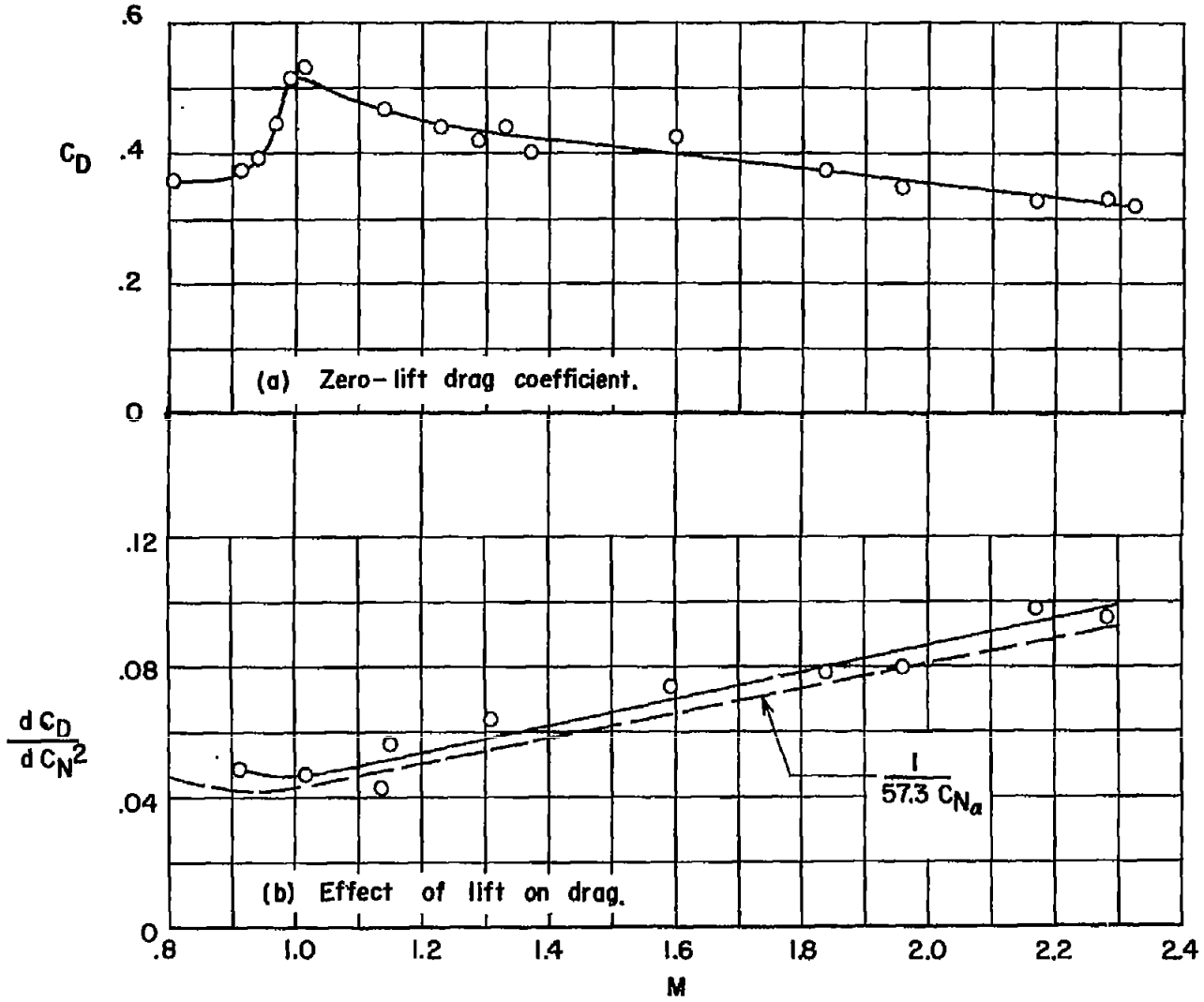

Figure 13.- Variation of zero-lift drag coefficient and drag due to lift with Mach number.

[redacted]

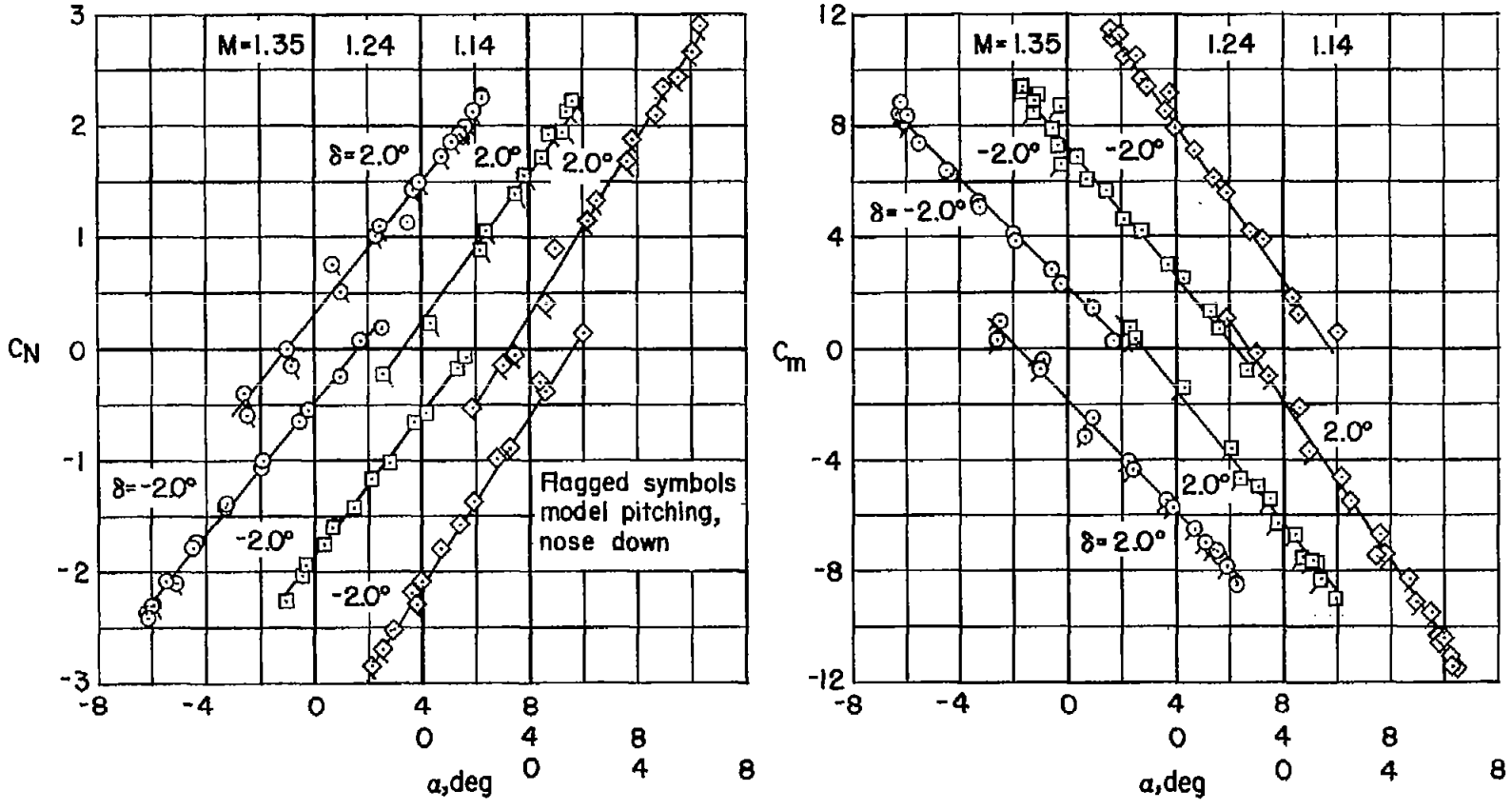

(a) First coasting period.

Figure 14.- Typical variation of normal-force and pitching-moment coefficients with angle of attack during symmetrical oscillations.

[redacted]

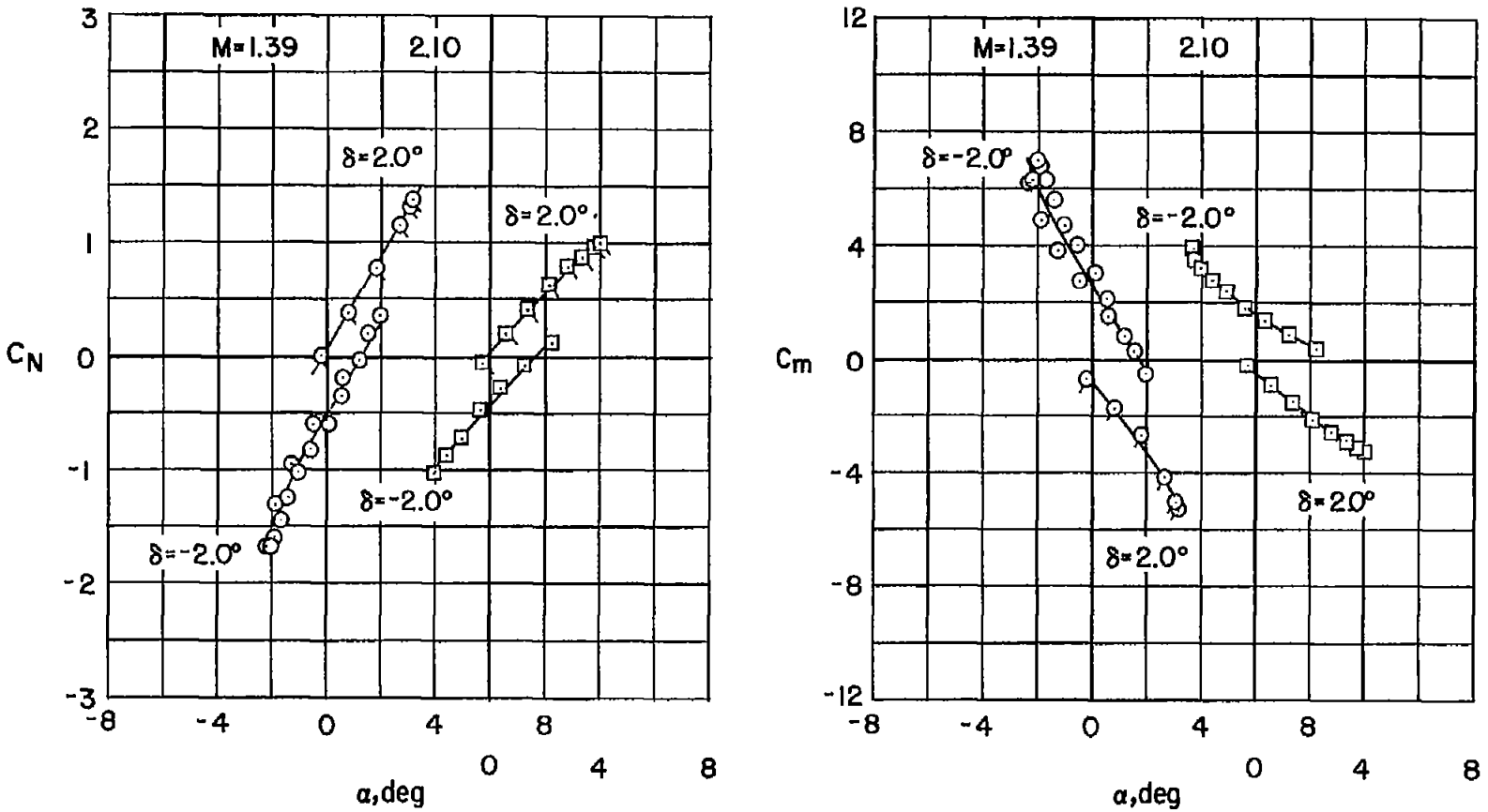

(b) Power-on flight.

Figure 14.- Continued.

[redacted]

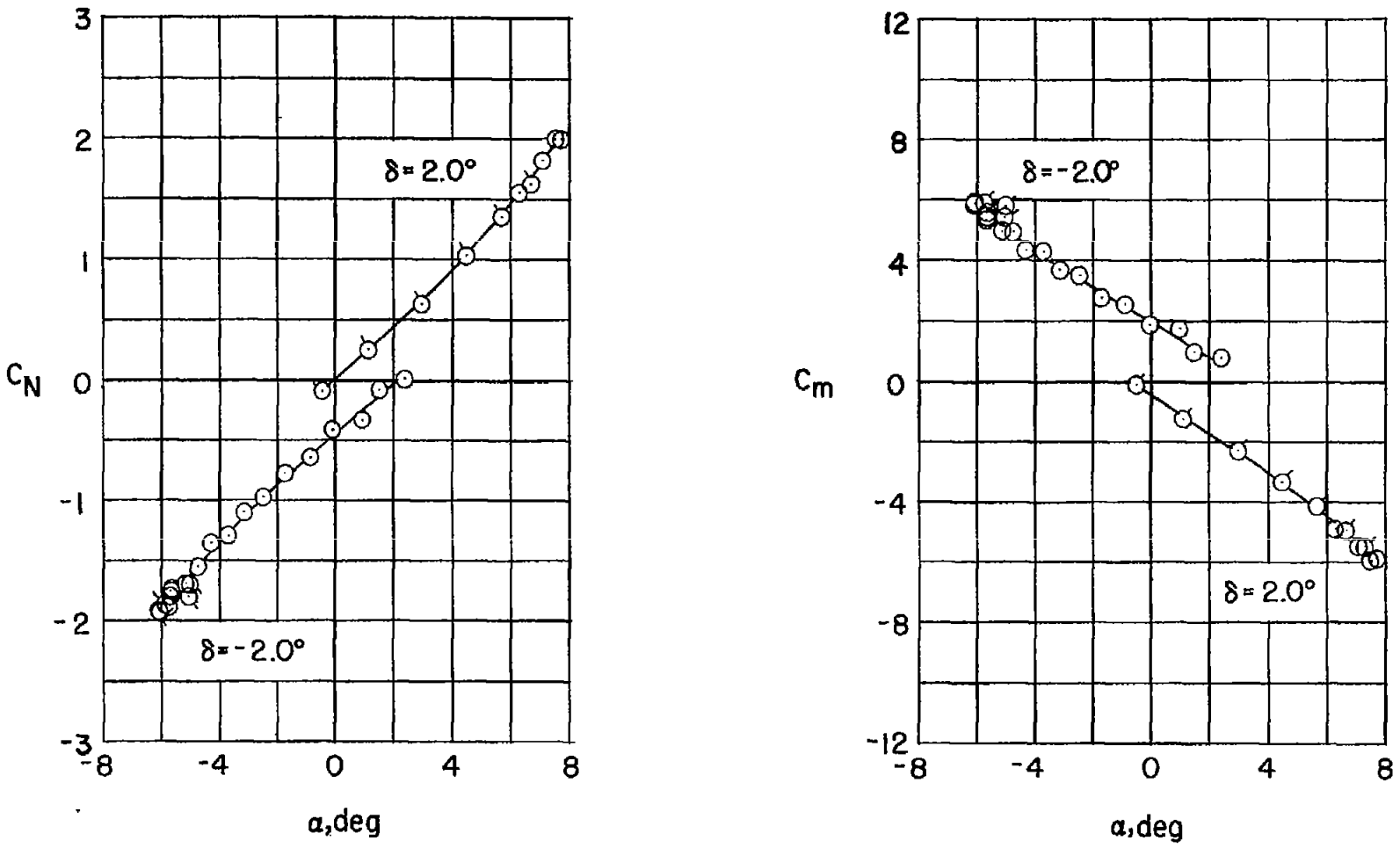

(c) Second coasting period. M = 1.90.

Figure 14.- Concluded.

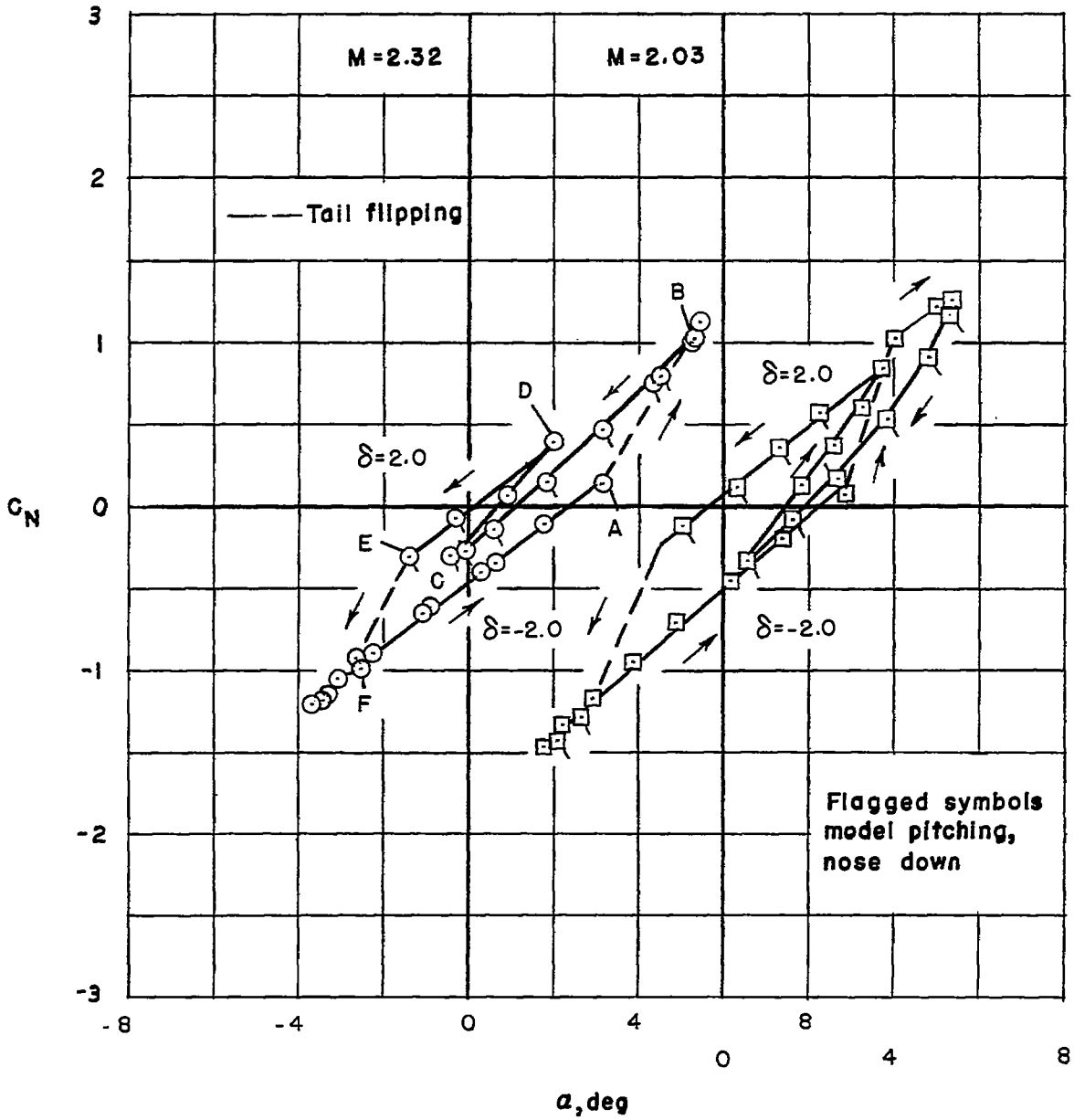

(a) Normal-force coefficient against angle of attack.

Figure 15.- Typical variation of normal-force and pitching-moment coefficients during asymmetrical oscillations of second coasting period.

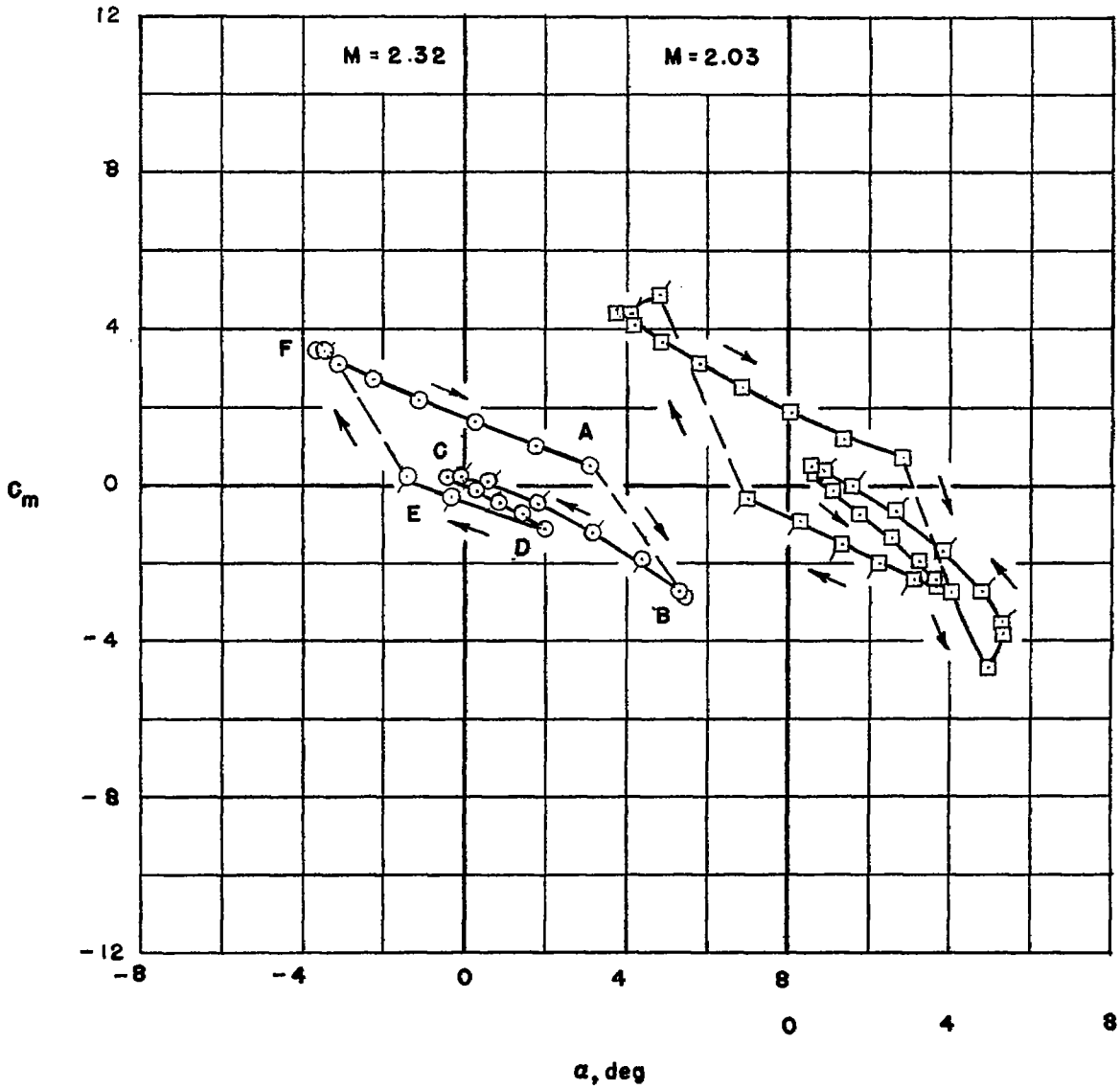

(b) Pitching-moment coefficient against angle of attack.

Figure 15.- Concluded.

[redacted]

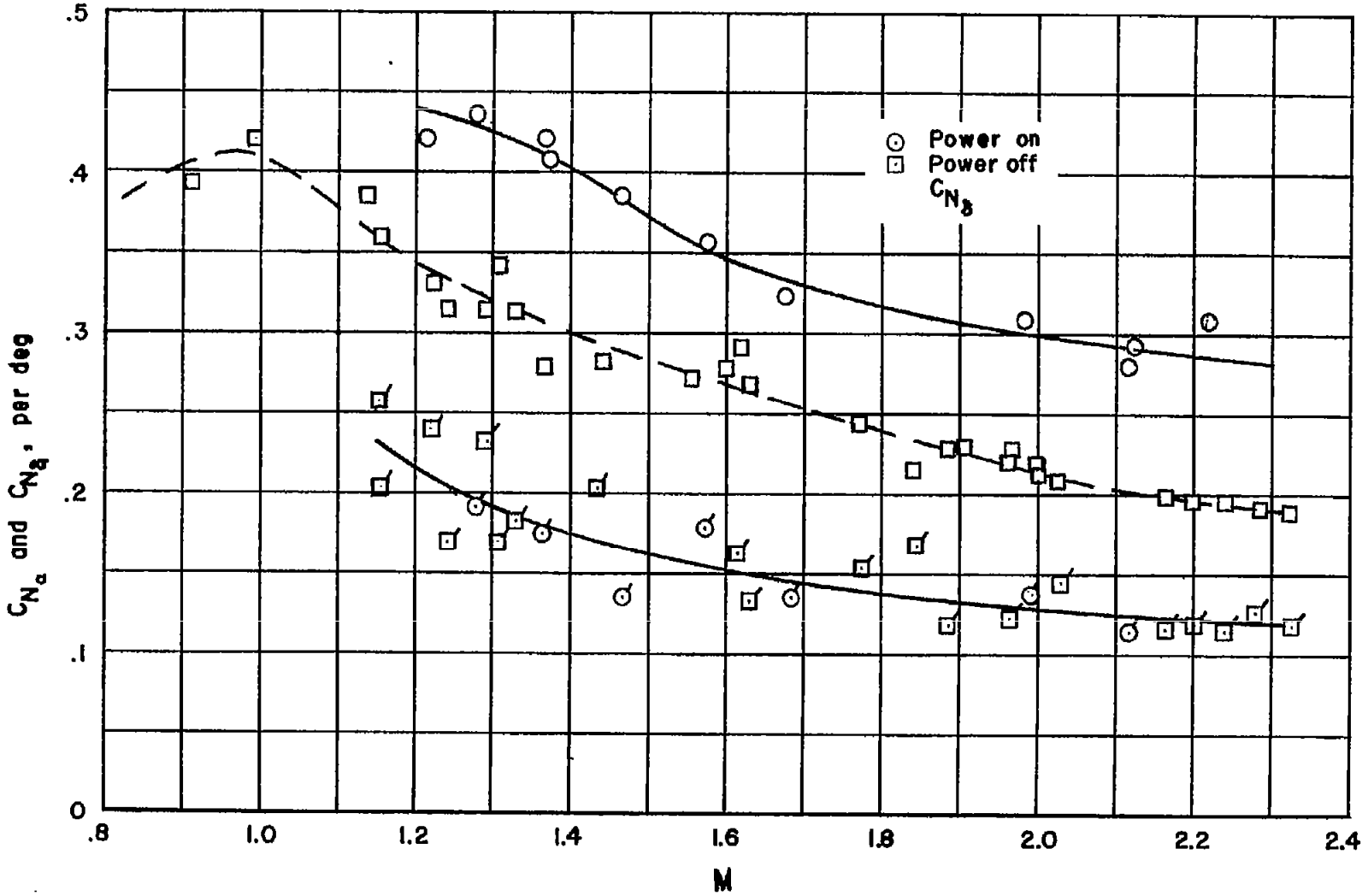

Figure 16.- Power-on and power-off values of C_{N_α} and C_{N_δ}.

[redacted]

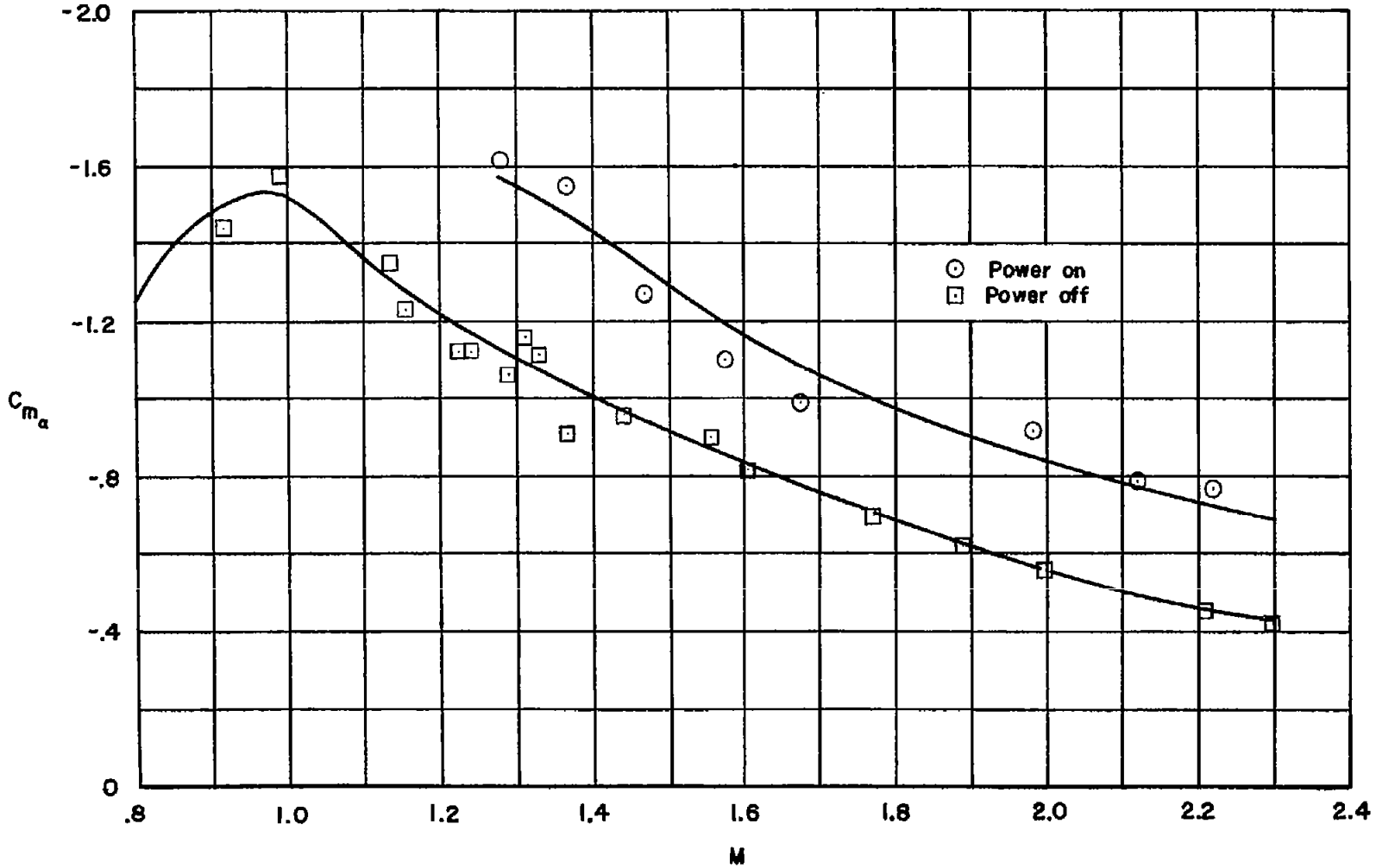

Figure 17.- Variation of pitching-moment-curve slope with Mach number.

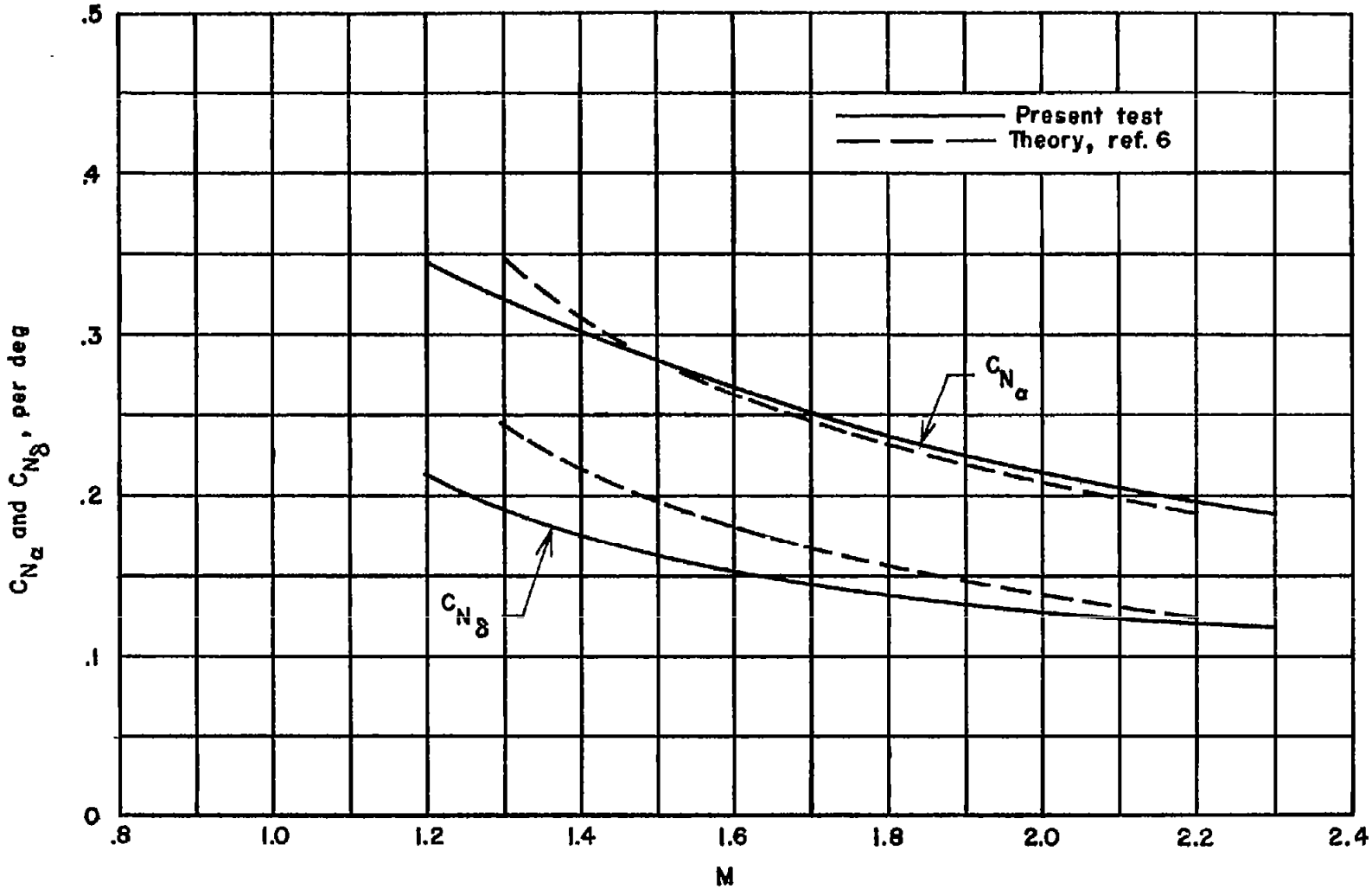

Figure 18.- Comparison of theory and experiment for C_{N_α} and C_{N_δ}.

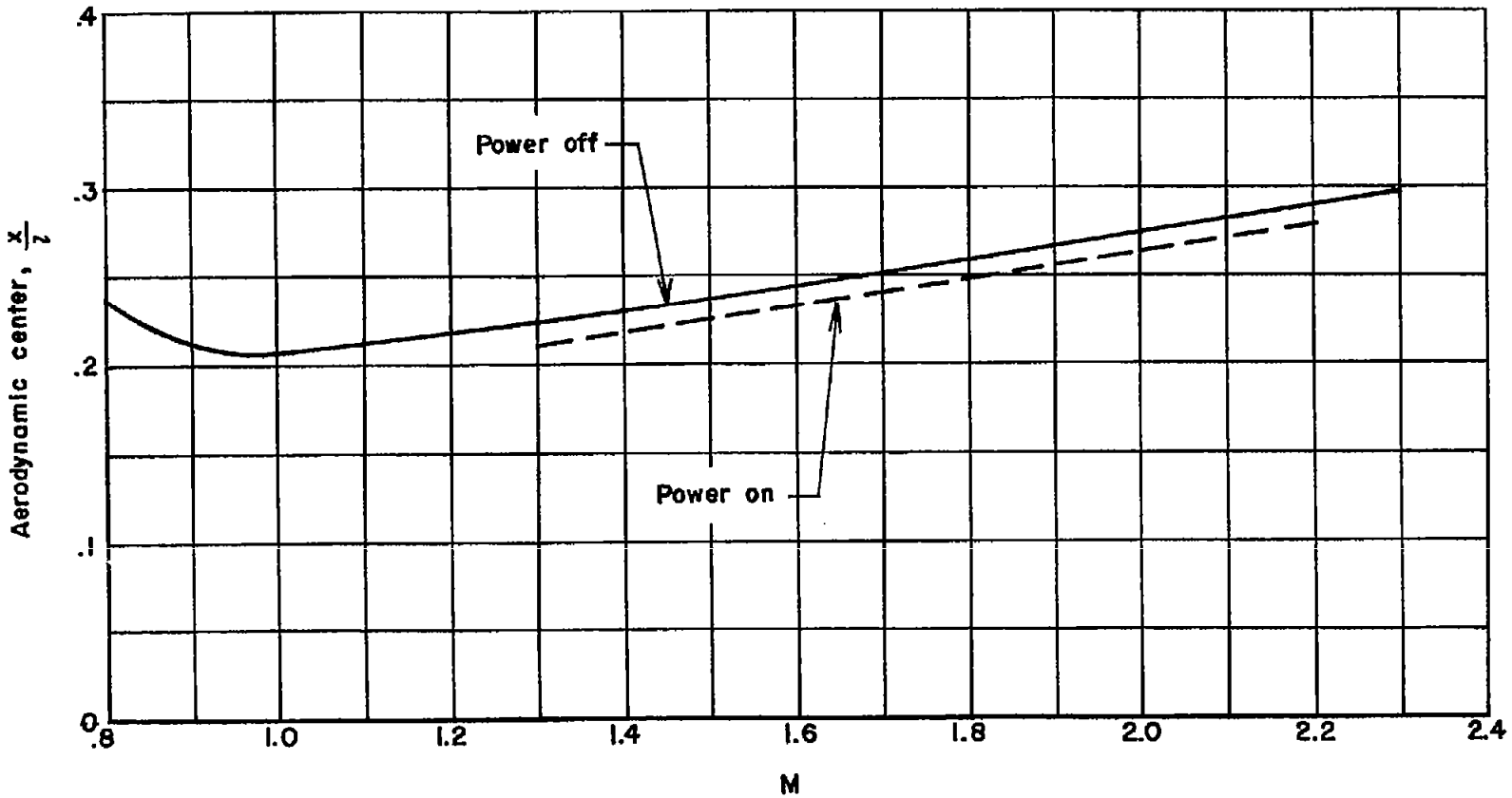

Figure 19.- Comparison of power-on and power-off aerodynamic-center locations.

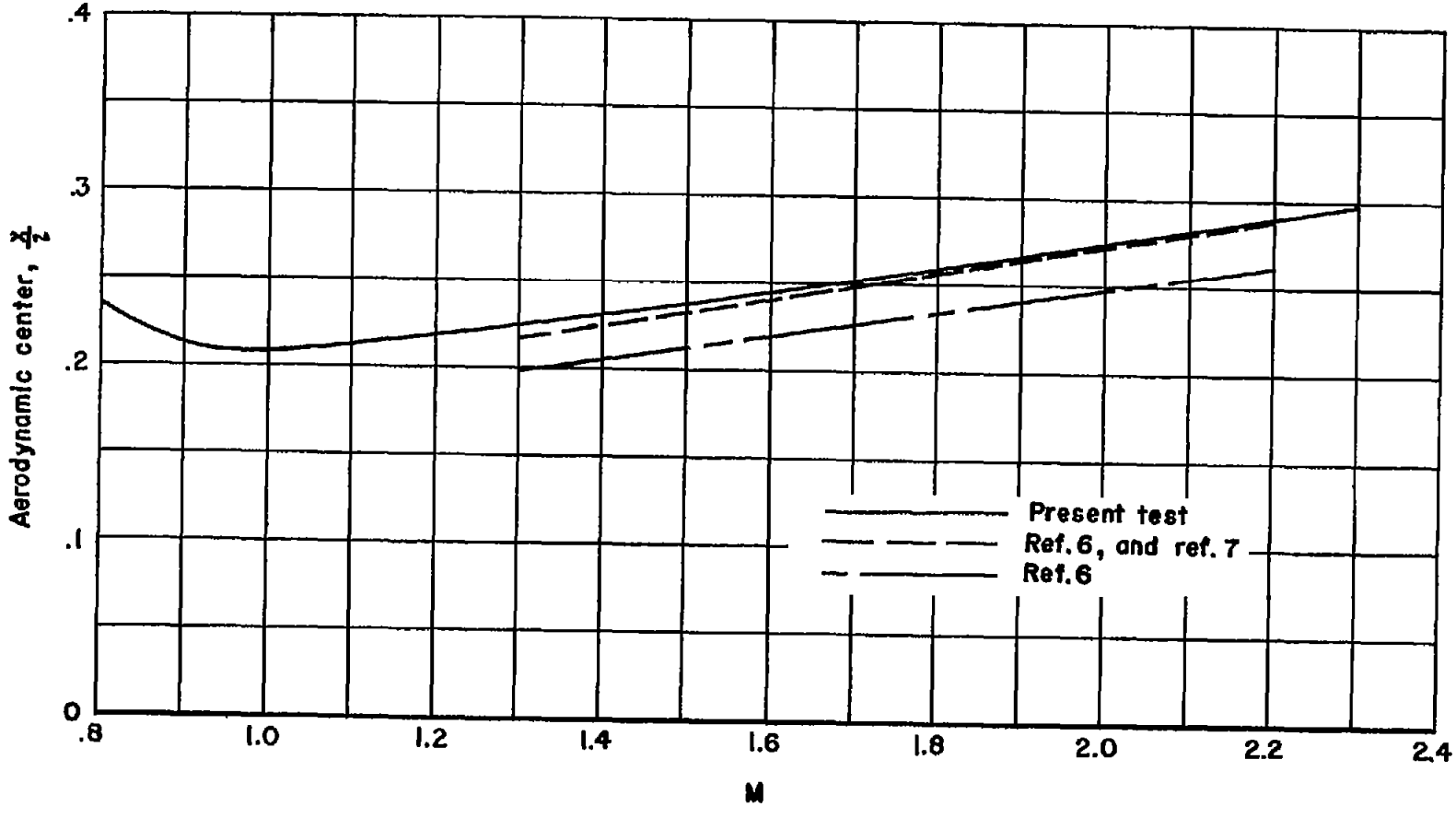

Figure 20.- Comparison of theory and experiment for aerodynamic-center location. Power-off flight.

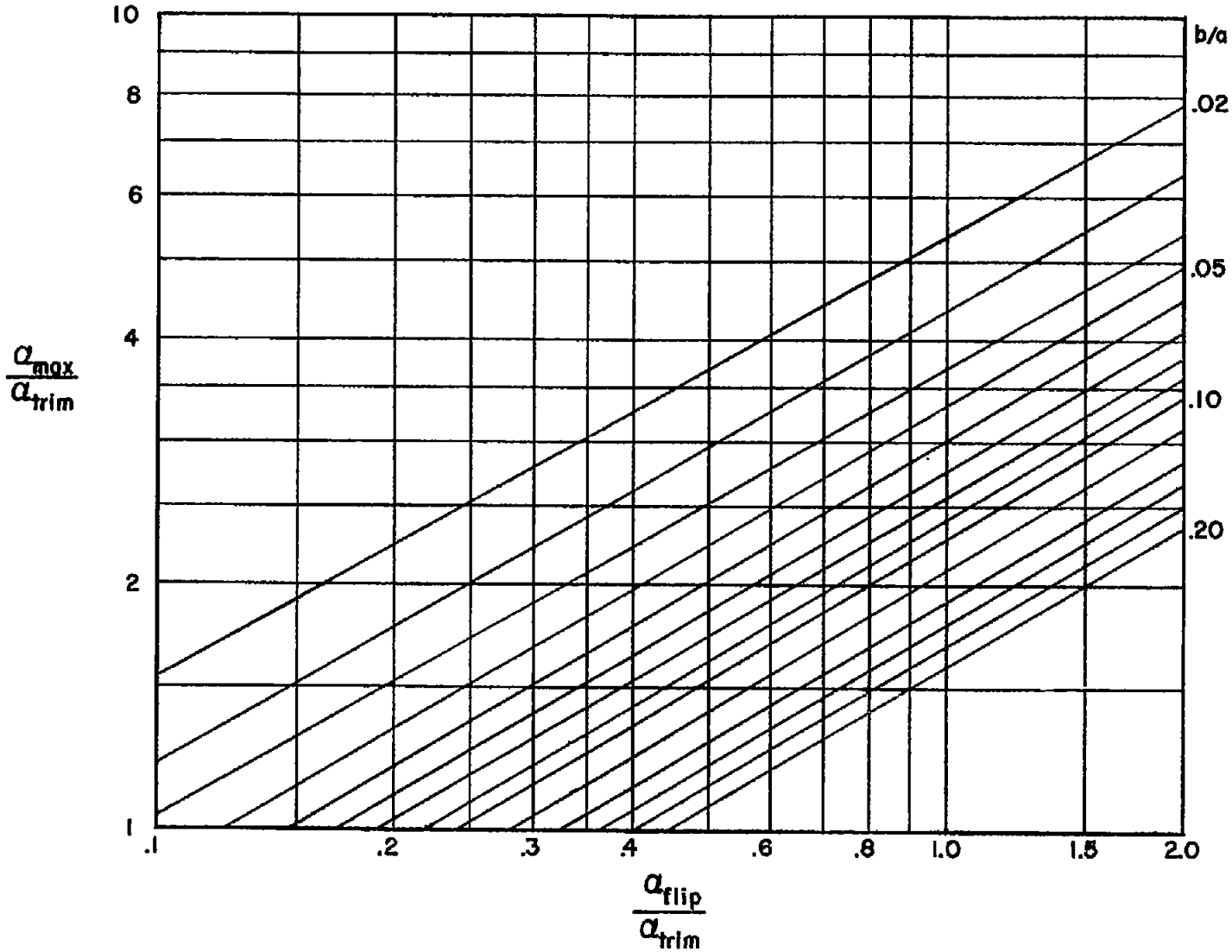

Figure 21.- Aeropulse response chart.